waterloopkundig laboratorium
delft hydraulics laboratory

a method of computation of unsteady wave-driven coastal currents

test-cases of RIPCEL

report on mathematical investigation

R 1174-8

October 1982

toegepast onderzoek
waterstaat

CONTENTS

TABLES

FIGURES

A METHOD OF COMPUTATION OF UNSTEADY WAVE-DRIVEN COASTAL CURRENTS; TEST-CASES

1. Introduction

In [12] a method is described of the computation of unsteady wave driven coastal currents. The objectives of this method, which is called RIPCEL, are also described in [12] and will be mentioned only briefly here:

a. the investigation of the instability and non-linear phenomena in longshore currents
b. the study of the importance of various processes in the surfzone
c. a validity check on simpler models.

After the construction of the model it seemed useful first to investigate the model results for various well-known situations. The results of this investigation are presented in this report. The phenomena which are studied are:

a. wave set-up
b. longshore currents
c. circulation currents near the shore
d. currents around breakwaters
e. currents in a closed basin

In a few situations also the transformation procedure of the numerical grid has been tested. Where possible a comparison with the analytical solution has been made. It may be pointed out that instead of optimizing the accuracy of the numerical results it was thought preferable to increase the number of different classes of problems. An investigation in depth can be carried out at a later stage.

The present investigation is part of a research programme "Coastal Investigations" sponsored by the Ministry of Transport and Public Works - Rijkswaterstaat, in which the Delft Hydraulics Laboratory and the Delft University of Technology participate.

The author, dr. H.G. Wind, acknowledges many helpful and stimulating discussions with Prof. dr. C.B. Vreugdenhil and the programming efforts of Mr. C. ten Napel.

2. Wave set-up

2.1 Description of the problem

The variation in mean water level caused by shoaling and breaking of waves has been explained by theory and confirmed qualitatively by experiments. In the present case regular waves, normally incidentto a plane sloping beach will be considered. Details about the geometry and wave conditions are presented in Table 1.

2.2 Analytical solution

The definition of the various variables is shown below.

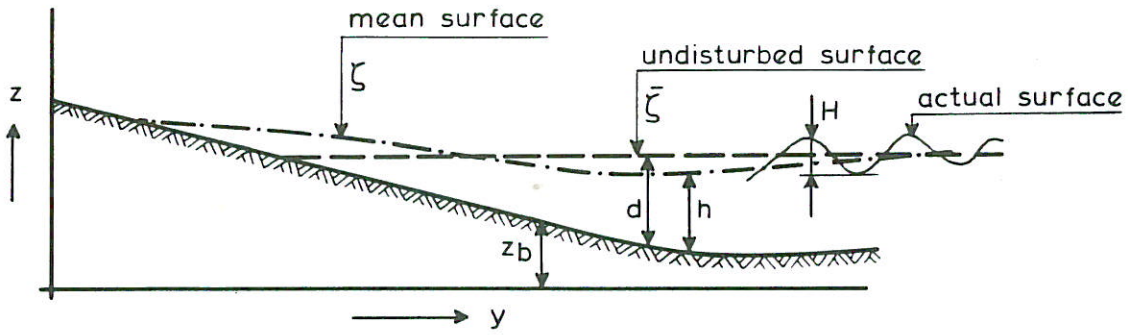

In most problems presented in this report the shoreline is straight and parallel to the x-axis.

In Appendix A of this report the complete equations are presented. For the problem under consideration the equation for the y-momentum reduces to

$$\frac{1}{\rho}\frac{\partial S_{yy}}{\partial y} + g\,(d + \bar{\zeta})\,\frac{\partial \bar{\zeta}}{\partial y} = 0 \qquad (2.1)$$

The definition of S_{yy} is also given in Appendix A. The solution for this equation is known in the case of a wave field determined on the basis of the following definition of the breaker index

$$\gamma = H/(d + \bar{\zeta}) \qquad (2.2)$$

However, $\bar{\zeta}$ is initially unknown in the present problem and hence (2.1) is sol-

ved analytically by using as a definition of the breaker index

$\gamma = H/d$.

The boundary condition in deep water is $\overline{\zeta} = 0$. The result of this computation is presented in Figure 1 as the analytical solution.

2.3 Numerical solution

The boundary condition near the shoreline is formed by a perfect reflecting boundary at a still waterdepth of 0.10 m. The position of this boundary has been chosen so that during the calculations the mean water depth at that point is always positive. For the construction of the seaward boundary great care has been taken to avoid reflections of this boundary. In this case the procedure proposed by Gustafsson and Sundström was followed. For details see [4]. For the boundary conditions of the sides normal to the shoreline periodicity has been assumed i.e. the velocity field repeats itself along the shore.

For the definition of the water depth at the seaward boundary, the wave set-down has also to be taken into account. In the present tests the following procedure has been followed. The wave conditions have been obtained using the still-water depth. The set-down at the seaward boundary has been calculated using the linear wave theory and assuming $\overline{\zeta} = 0$ at infinity. For the calculations of the wave set-up the still-water depth has been reduced with the set-down calculated at the seaward boundary.

Details of the finite difference grid are presented in Table 2. The mean water level due to shoaling and breaking of the waves is presented as the numerical solution in Figure 1.

2.4 Discussion

Inherent to the approach is that the set-down at the seaward boundary is equal for both methods. Progressing in shoreward direction, small differences between both methods appear. Near the shoreline the numerical solution is marginally, but consistently lower than the analytical solution. It is thought that this is caused by numerical inaccuracies. In general the agree-

ment between the analytical and the numerical solution is satisfactory. Time functions of the onshore-offshore velocity for three points are presented in Figure 2. The first point is located 10 m offshore, the second point is found at the breaker line, while the last point is positioned at the seaward boundary 100 m offshore. The initial wave generated by the sudden application of the gradients in the radiation stress can be seen clearly. Inside the breaker zone this causes a flow in onshore direction, while near the seaward boundary the flow is directed in offshore direction. After the reflection of the initial wave against the beach the wave runs out of the system. The reflection of the wave against the seaward boundary can hardly be noticed from Figure 2. This means that the proposed conditions indeed yield a weakly reflecting boundary.

3. Longshore current

3.1 Description of the problem

The examples of wave driven longshore currents treated in this chapter are restricted to regular waves, obliquely incident to an infinite long plane beach.

3.2 Analytical solution

Longuet Higgins (1970) has given the analytical solution of the problem mentioned above. The solution is summarized in Appendix B. An important parameter in this solution is the factor P. This factor P represents the ratio between the coefficient of the dimensionless lateral mixing term and the coefficient of the dimensionless bottom friction term:

$$P = (\pi\ m\ N)/(\gamma.C) \tag{3.1}$$

m = combined slope of the beach and mean water level $(\frac{\partial d}{\partial y} + \frac{\partial \bar{\zeta}}{\partial y})$
N = viscosity coefficient (0.01)
C = bottom friction coefficient (0.01)
γ = breaker index $(H/(d+\bar{\zeta}))$

For m equals 0.025 and a breaker index of 0.8 the resulting value for P is 0.098.
In Figures 3 and 4 the analytical longshore current profile is shown respectively for non-viscous flow (N = 0) and for viscous flow (N = 0.01). The boundary condition at the shoreline and at the seaward boundary is v = 0.
If it is assumed that the boundary layer develops within one grid spacing from the shoreline, the free slip condition can be applied:

$$\frac{\partial}{\partial y}\ (p/h) + \frac{\partial}{\partial x}\ (p/h) = 0 \tag{3.2}$$

The analytical solution for the wave driven longshore current, using the free slip condition and similar approximations as in Longuet Higgins (1970), has been derived in Appendix B. The resulting velocity profile is shown in Figure 5. The similarity between Figures 4 and 5 is striking. This implies that the choice of boundary condition has in this case only a local effect.

3.3 Numerical solution

Information about the grid is given in Table 2. In this example use has been made of the grid transformation procedure. The grid spacing increases in offshore direction. In this way the grid points are concentrated in the interesting area.

In Figures 3 and 5 the numerical solutions are shown for the wave driven longshore current at T = 200 s and T = 800 s. In Figure 3 the fluid flow is non-viscous (N = 0), while in Figure 5 the viscosity constant N = 0.01. The resulting value for P is P = 0.098. The boundary condition in both cases is the free slip condition (3.2). In Figure 4 the wave driven longshore current is presented for P = 0.098 and the boundary condition v = 0 at the most shoreward grid point.

The time function of the current velocity at the breakerline for P = 0 and P = 0.098 is shown in Figure 7. From this Figure it is clear that after T = 800 s the velocity is almost constant and only minor changes are to be expected with the increase in time.

3.4 Discussion

The difference between the numerical and analytical solution in Figures 4 and 5 is smaller than 6%. In Figure 3 the agreement between both methods is better except for the velocity at the breakerline. The velocity at the breakerline is reduced because of the smoothing of the infinite velocity gradient at the breakerline. In general the agreement is satisfactory.

A difference between the analytical model and the numerical model concerns the position of the boundaries. In the analytical model the shoreward boundary is located at the mean water line, while in the numerical model this boundary is positioned at a distance from the shore of about 0.05 times the width of the breaker zone (Y/YB = 0.05). The seaward boundary in the analytical model is at infinity, whereas this distance in the numerical model is restricted to two to four times the width of the breakerzone (see Table 1). The effect of the position of the boundaries on the velocity profile has been investigated using the analytical solution that is given in Appendix B. The result of this analysis is shown in Figure 6. In the graph on the top of Figure 6 the shoreline is positioned at the mean water line, while the position of the seaward boundary has

been varied between Y/YB = 1.1 and Y/YB = 2.7. For each position of the seaward boundary the dimensionless longshore current velocity has been calculated, using the analytical solution in Appendix B in the following points

V0.1/V0 = velocity at Y/YB = 0.1
V0.6/V0 = velocity at Y/YB = 0.6
VB/V0 = velocity at the breaker line
Vsea/V0 = velocity at the seaward boundary

This information is shown in Figure 6. To this Figure also the dimensionless velocities have been added with the position of the seaward boundary at Y/YB = ∞. From the graph at the top of Figure 6 can be seen, that if the seaward boundary is located at a distance from the shore of at least 1.5 to 2 times the width of the breaker zone, the velocity profile inside the breaker zone is not influenced by the position of the seaward boundary. For a proper representation of the velocity at the seaward boundary this distance may even increase to 3 times the width of the breaker zone.
In the graph at the bottom of Figure 6 the effect of the position of the shoreward boundary on the velocity profile has been investigated. The seaward boundary has been located at infinity. For a variation of the shoreward boundary at distances between Y/YB = 0.05 and Y/YB = 0.25 the dimensionless velocities have been calculated at the following points, using the analytical solution in Appendix B.

V-Boundary/V0 = velocity at the shoreward boundary
V0.6/V0 = velocity at Y/YB = 0.6
VB/V0 = velocity at the breaker line

To Figure 6 also the dimensionless velocities have been added, with the shoreward boundary positioned at the mean water line. The conclusion that can be drawn from Figure 6 is that the position of the shoreward boundary only influences the dimensionless velocity at the shoreward boundary. The peak velocity at Y/YB = 0.6 is not influenced by the position of the shoreward boundary.
The conclusion of this analysis is, that the differences between the analytical and numerical peak velocities in Figures 3 through 5 are not caused by the differences in the position of the boundaries in both approaches.

For certain practical conditions it is sometimes proposed to neglect terms

which are much smaller than other terms in the equation. According to the P-value of 0.098 the viscosity term is indeed much smaller than the bottom friction term. However, the longshore current profile is a good example of what the effects are on the shape of the profile when the highest order terms in the equations are neglected, even if these terms are relatively small.

4. Circulation currents

4.1 Description of the problem

The momentum equations for the circulation currents are restricted to motions in the horizontal plane, because of the averaging over the depth. A well known problem is that of circulation currents resulting from a perturbation of the set-up generated by normal incident waves. Attempts to solve this problem have been made by Hino (1974), Le Blond and Tang (1974) and Miller (1977). Although RIPCEL in principle is well suited to tackle this type of problem, the present study will be restricted to forced circulations. This type of circulations is induced by a longshore variation in wave height. Such a variation can be caused by a combination of an oblique incident wave fieldwith a wave field reflected from e.g. a structure (Liu and Mei, 1974) or by a combination of two incident wave fields (Dalrymple, 1975).

4.2 Analytical solution

An analytical solution of the forced circulation currents is given by Bowen (1969). He assumes in the breakerzone a normal incident wave field with the following wave height distribution:

$$H = \gamma m\bar{y} \ (1 + \xi \cos \lambda x) \qquad \xi << 1 \qquad (4.1)$$

ξ = perturbation parameter
$\lambda = 2\pi/L_o$
L_o = wave length of the perturbation

In the analytical solution the bottom-friction is defined as:

$$\frac{1}{\rho} \ (r_{bx}, r_{by}) = c(u,v) \qquad (4.2)$$

where
$c = 0.01$.

The breaker index γ equals

$$\gamma = H/(d + \bar{\zeta}) \qquad (4.3)$$

The longshore variation of the bottom topography is such that γ = constant.

The solution given by Bowen (1969) can inside the breaker zone be written as

$$u = \frac{\lambda}{(h+\bar{\zeta})} \sin \lambda x \left[P\, s \sinh s + \frac{Bm^2}{c\lambda^4} 2s.(\cosh s - 1) \right] \tag{4.4}$$

$$v = -\frac{\lambda}{(h+\bar{\zeta})} \cos \lambda x \left[P(s \cosh s - \sinh s) + \right.$$

$$\left. + \frac{Bm^2}{c\lambda^4} \{2 - s^2 + 2s \sinh s - 2 \cosh s\} \right] \tag{4.5}$$

and outside the breaker zone:

$$u = \frac{\lambda}{(h+\bar{\zeta})} \cdot \sin \lambda x \cdot Q.s\, e^{-s} \tag{4.6}$$

$$v = -\frac{\lambda}{(h+\bar{\zeta})} \cos \lambda x \quad Q(s+1)e^{-s} \tag{4.7}$$

where:

$$s = 2\pi y/L_o \tag{4.8}$$

The coefficients P and Q have to be determined in such a way that the basic stream function of (4.6) through (4.7) and its derivative normal to the breaker-line $\frac{\partial \psi}{\partial y}$ are continuous. For the conditions mentioned in the Tables 1 and 2 the analytical solution is shown in Figure 8. In this solution the no-slip condition (u=0) has been assumed at the shoreline. In the numerical solution for viscous flow the free-slip condition (3.2) applies.

An analytical approximation of the velocity field outside the breaker zone can be obtained if $y_b \geq \frac{1}{2}L_o$. In that case the hyperbolic functions reduce to simple exponential functions and the following velocity field outside the breaker zone results.

$$u = -\frac{1}{8} \frac{g\, \gamma^2\, m^2\, \xi}{c.\lambda} \cdot (s_b - 2) \quad e^{(s_b - s)} \sin \lambda x \tag{4.9}$$

$$v = \frac{1}{8} \frac{g\, \gamma^2\, m^2\, \xi}{c.\lambda} \cdot \frac{(s_b - 2)(s+1)}{s} e^{(s_b - s)} \cos \lambda x \tag{4.10}$$

For the analysis of the momentum equations a reference velocity is required. A possible choice is the outflow velocity v at the centre of the rip current at the breakerline:

$$v = \frac{1}{8}\,\frac{g\,\gamma^2\,m^2\,\xi}{c.\lambda}\,.\,\frac{(s_b-2)(s+1)}{s} \qquad (4.11)$$

Inside the breaker zone the condition $y \geq \frac{1}{2}L_o$ is not always satisfied and therefore a similar approximation as in (4.9) and (4.10) cannot be obtained there.

4.3 Numerical solution

Bowen (1969) has assumed that the shallow water approximations of the linear wave theory apply inside the breaker zone. In the present example a breaker height of 1.10 m and a perturbation $\xi = 0.1$ has been assumed. The longshore wave length of the perturbation is $L_o = 200$ m. This wave field has been matched with a wave field outside the breaker zone using a long wave (T = 25 s). Such a long wave period has been assumed, because it was initially expected that the longshore variation in mean water level at the seaward boundary caused by the longshore variation in wave height had to be minimized because this could be a possible source of numerical problems. Later this appeared not to be so. Only for the calculation of the circulation cells as presented in Figure 9 the bottom friction defined by Bowen has been used with c = 0.01. For the remaining cases the approximation of Longuet Higgins (1970) have been applied (see also [12]).
The effect of the longshore variation in bottom topography on the current field has been neglected. This is in agreement with the solution of Bowen (1969).
In the analytical solution two symmetrical cells are given. The numerical solution results in two symmetrical cells as well. However, in order to reduce the computation time only one cell bordered by two side walls has been computed. Along these side walls the same conditions apply as along the shoreline. Details of the grid size, time step etc. are given in Table 2.

The following calculations have been carried out.

Figure no.	bottom friction	viscosity factor N	convective terms	comments
8	yes	0	no	
9	yes	0	no	analytical solution
10	yes	0.01	no	Re = 0
11	yes	0	yes	Re = ∞
12	yes	0.01	yes	Re = 3
13	no	0.01	yes	Re = 3
14	no	0.01	yes	Re = 9 increased driving force
15	no	0.0033	yes	Re = 9 original driving force
16	yes	0	yes	curved shoreline

The Reynolds number is defined in Paragraph 4.4.

4.4 Discussion

In Figures 8 and 9 the analytical solution and the numerical representation of the Bowen cells are presented. At first sight the agreement is fair. A closer look however reveals that the difference in boundary condition near the shoreline is hindering a more quantitative comparison in that area. For a check on the accuracy of RIPCEL this type of calculation should be repeated at a later stage of this research, but with a no-slip condition at the shoreline. In Figure 10 the same configuration is presented but now viscosity has been added, with N = 0.01. In Figure 11 the effect is shown of including the convective terms instead. In Figure 12 the combined effect of all terms e.g. bottom friction, lateral mixing and convective terms can be seen. A comparison of Figures 9 through 12 learns that the differences are rather small. This point becomes clear if the momentum equations are made dimensionless by a reference velocity U_o and a length L_o. From these dimensionless equations parameters can be obtained which express the relative importance of the various terms

$$Re = \frac{\text{convective term}}{\text{viscous term}} = \frac{U_o}{m^{\frac{1}{2}}\ g^{\frac{1}{2}}\ L_o^{\frac{1}{2}}\ N} \qquad (4.12)$$

$$P = \frac{\text{viscous term}}{\text{bottom friction term}} = \frac{\pi\ m\ N}{\gamma . c} \qquad (4.13)$$

The parameter P has been derived by Longuet Higgins (1970) in his study on longshore currents. The product of Re and P gives the importance of the convective term relative to the bottom friction term.
The reference velocity U_o will be chosen to be the velocity in the centre of the rip current in a Bowen cell (4.11). For the reference length L_o the longshore wavelength of the perturbation has been chosen.

For the present conditions these assumptions lead to a Reynolds number of 3 and a value of P = 0.1. From the value of P it follows that the viscosity terms are ten times smaller than the bottom friction terms. From the Reynolds number it follows that the convective terms are more important than the viscosity terms, but from the product of Re and P it can be seen that these terms are still small relative to the bottom friction terms. This implies that the present condition to a large extent is dominated by bottom friction and that indeed the differences between the Figures 9 through 12 ought to be small.
One point in which the Figures 9 and 10 differ from the Figures 11 and 12 is that in the latter two Figures there appears to be a shift to the right of the centre of the cell. This mechanism has been pointed out by Arthur (1962). He has shown that conservation of vorticity along a streamline leads to a narrowing of the streamline pattern of a current flowing into deeper water.

In Figure 13 the bottom friction has been made zero. Both convective terms and lateral mixing are active. The driving forces remaining the same, this obviously must lead to an increase in velocity. The vorticity remaining the same (as in Figure 12) no further shift of the centre of the cell is observed. This is as one would expect from the argument mentioned above.

There are two ways of changing the Reynolds number: the first one by changing the viscosity coefficient N and the second by changing the driving forces. Bowen (1969) used the latter approach. This implies for the present case a change in vorticity and, from the conservation of vorticity, a change in the position of the centre of the cell. This would mean that the suggestion by Bowen that the shape of the cell is a function of the Reynolds number is not quite true. The changes in the cells as presented by Bowen are caused by the change in the input vorticity.

To illustrate this point two types of calculations have been made. In the first calculation the perturbation ξ of the longshore variation in wave height is

increased by a factor of 3. This implies an increase in driving force by a factor of 9. The result is shown in Figure 14. Except the increase in the velocity by roughly a factor of 3, it can clearly be seen that the cell centre in Figure 14 has moved to the right relative to the position in Figure 13 (Re = 3). However, in Figure 15 the Reynolds number has been raised by reducing the coefficient N for lateral friction by a factor of 3. In Figure 15 can be seen that this Re = 9 case is almost indistinghuishable from the Re = 3 case (Figure 13). This confirms, that the viscosity effect is small relative to the convective effect (high Reynolds number).
This calculation is also a demonstration of the point that for the present cases the degree by which the distance between the streamlines are reduced depends on the vorticity and not on the Reynolds number.

At first sight also a different conclusion could be drawn from a comparison of the Figures 13 and 15. This conclusion is that in fact the numerical viscosity is much larger than the physical viscosity. This implies that in that case the real Reynolds numbers in Figures 13 and 15 are in the order of 0.3 or even smaller. It must be borne in mind that a flow with low Reynolds number (Re= 0.1) is dominated by viscous effects, while flows with a high Reynolds number are dominated by convective effects. For a stationary flow in a given geometry the drag of a viscous flow changes linearly with the velocity, while the inertia of the convective flow changes with the square of the velocity. From the flow field in Figure 15 compared with the flow field in Figure 13 it is clear that the change of the driving force by a factor of 9 only resulted in a change in velocity by a factor of 3. This shows that the present flows are dominated by convective effects and not by viscous effects. This implies that the numerical viscosity is at most of the same order of magnitude as the physical viscosity.

In Figure 16 an example is given of an application with a curved shoreline. The grid and the equations are generated by taking into account the transformation functions. A comparison between Figures 11 and 16 shows that the flow field has only changed marginally. At a later stage of the research the transformation procedures will be further investigated.

For this example also the solution speed of the programme has been checked. It appears that RIPCEL takes 1 computer second on a Cyber 175 to treat 175 points. This is somewhat slow relative to comparable programmes.

5. Currents around breakwaters and in basins

5.1 Description of the problem

The study of the importance of various processes in e.g. currents around breakwaters and in basins is one of the objectives of the development of RIPCEL. This chapter will be restricted to cases which will clearly reveal probable problem areas. This will be the case for currents in which viscous damping is absent.
Furthermore a very simple wave field will be used, namely it is assumed that the oblique incident wave field (30^{o}) runs through the breakwaters, i.e. diffraction effects will be neglected. This point can be improved at a later stage by use of existing refraction-diffraction programmes, without changing RIPCEL essentially. Bottom friction and lateral mixing are modelled as proposed by Longuet Higgins (1970) in case of longshore currents. The geometry is a gently sloping plane beach (1:40) with a breakwater extending to 70 m or 200 m offshore.This last case essentially represents a closed wave basin. The distance between the breakwaters is 100 m. Further details about the geometry and the wave field are given in Table 1.

5.2 Numerical solution

Information about the grid can be found either in Figures 17 and 18 or in Table 2.
The boundary conditions are the same as for the circulation cells, except for the breakwaters. In principle the breakwater is impermeable to currents. As a boundary condition it has been assumed that the velocity normal to the breakwater is zero. Along the boundary, seaward of the breakwater, initially periodic boundary conditions were assumed. However, this led to a solution in which the offshore transport q became zero at the head of the breakwaters. This caused an undulating velocity profile along the breakwaters. After some experiments the following rough solution has been adopted. At the head of the breakwater it is assumed that p and q are different at both sides of the breakwaters, but h is periodic. At the first shoreward point all three components differ on both sides of the breakwater. At the first seaward point of the head of the breakwaters q and h are periodic, but p is free. At the second seaward point all three components are periodic. This solution appeared to yield reasonable, but not optimal results.

The requirements for stability and accuracy of the numerical scheme are presented in [12]. A few of these requirements are recalled here. First of all the stability of the implicit scheme is guaranteed if

$$\Theta \geqslant \tfrac{1}{2}$$

The second condition is that the cell Reynolds number must be smaller than 2 in areas of strong velocity gradients

$$R_{\Delta x} = U.\Delta x/\varepsilon < 2$$

This number determines the grid spacing.

An estimate of the numerical viscosity is (see [12])

$$\varepsilon_{num} \simeq (\Theta - \tfrac{1}{2}) \; . \; \Delta t \; . \; gh \qquad (5.1)$$

This numerical viscosity must be compared with a first estimate of the physical viscosity made by Longuet Higgins (1970)

$$\varepsilon_{phys} = N \; . \; g^{\frac{1}{2}} \; h^{3/2} \; /m \qquad (5.2)$$

where m is the bottom slope and N is a constant. The condition that $\varepsilon_{num} << \varepsilon_{phys}$ everywhere in the field leads to constraints on Θ and on Δt. On the one hand it was found that increasing the time step in the steady state indeed caused an increase in the numerical viscosity which could be seen from a reduction in the velocities.
On the other hand it was found that in some cases spatial oscillations occurred when the cell Reynolds number became too high. In principle the accuracy and stability must be further investigated in a later stage.

For the present conditions a time step of 4 s and $\Theta = 0.7$ have been chosen. After 100 s calculations have been terminated. Although the stationary solution may not completely have been obtained, the specific features of the solutions will be clear. The results are presented in Figures 17 and 18.

5.3 Discussion

At first sight there may appear to be some similarity between the circulation

cells in Figures 17 and 18 and the cells in Figures 8 through 16. The cells in Figures 17 and 18 however, are generated by oblique incident waves, i.e. by the term $\partial S_{xy}/\partial y$ whereas the cells in Figures 8 through 16 are generated by $\partial S_{xx}/\partial x$ and the longshore gradient in set-up caused by longshore gradient in $\partial S_{yy}/\partial y$. Looking from the breakerline in shoreward direction it can be seen that in case of oblique incident waves (Figure 18) the longshore velocity reduces much faster than in case of longshore variation in wave height (Figure 9). Near the shoreline the direction of the velocity even changes of sign. It is thought that part of this velocity is caused by a change in mean water level, which in its turn is induced by the deceleration of the longshore current by the breakwater. In Figures 8 through 16 this effect does not show up because if such a return current would build up, this current would be strongly counteracted by the high velocities in the nearshore area.

A comparison of the velocity fields around the breakerline in Figures 17 and 18 shows that differences are almost indistinguishable. This means that the present example the modelling procedure of the head of the breakwater does not influence this part of the velocity field.

From the head of the breakwater in seaward direction in Figure 17 the increasing periodicity in p and q may be noted clearly.

In order to be able to judge whether the results of RIPCEL are realistic a comparison with laboratory or prototype data is required. In that case the wave field in RIPCEL must include effects of the breakwaters, the set-up and possibly currents. This has not been done yet.

6. Conclusions and recommendations

The agreement between the analytical and numerical solution of the wave set-up and longshore current velocity profile is satisfactory. Qualitatively the numerical solution of the circulation current is comparable with the analytical solution. A closer comparison is not possible because of differences in boundary conditions.

The seaward boundary acts as a weakly reflecting boundary (Figure 2). Differences between the no-slip and free-slip condition along the shoreline disappear after a relative short distance from the shore (Figure 6). The effect of the position of the boundaries on the longshore current profile is marginal as long as the shoreward boundary is within 0.1 YB from the shore and the seaward boundary is located at 2YB from the shore (Figure 6).

For a proper choice of Δt, Θ and grid spacing a further investigation into the magnitude of the numerical viscosity and the effect of the cell Reynolds number must be carried out. After concluding this research the model can be used to study the stability of the set-up and the generation of rip currents. This topic is important for the reproduction of wave driven longshore currents.

The velocity distribution along the boundaries (Figure 17) may not be independent of the way in which the head of the breakwater is modelled. In case of a detailed investigation of the current pattern around the head of the breakwater this point must be clarified. A comparison of Figures 17 and 18 shows that the velocity field shoreward of the breakerline is not influenced by the way in which the head of the breakwater is modelled.

A comparison with laboratory and/or field data is required in order to check the validity of the model.

7. Notation

a	wave amplitude	m
c_f, C	frictional coefficient	-
d	undisturbed water depth	m
E	potential energy per unit area	Nm^{-1}
g	acceleration due to gravity	ms^{-2}
h	water depth	m
H	wave height	m
k	wave number	m^{-1}
L	length of region	m
m	beach slope	-
n	shoaling coefficient	-
N	coefficient in eddy viscosity	-
p,q	volume transports per unit width in x and y direction	m^2s^{-1}
P	viscosity-friction ratio	-
r	frictional parameter	ms^{-1}
Re	Reynolds number	-
$R_{\Delta x}$	cell Reynolds number	-
S_{xx} etc	radiation stress	Nm^{-1}
t	time	s
T	wave period	s
u,v	velocity components	ms^{-1}
x,y	horizontal coordinates	m
z	vertical coordinate	m
z_b	bottom level	
γ	breaking index	-
Δt	time step	s
$\Delta x, \Delta y$	mesh-widths	m
ε	eddy viscosity	m^2s^{-1}
η	water level variation due to waves	m
θ	weighing coefficient in difference scheme	-
λ	2π/wave length of perturbation	m^{-1}
ζ	water level relative to undisturbed level	m
ρ	fluid density	kgm^{-3}
τ_{bx}, τ_{by}	components of bottom shear stress	Nm^{-2}
τ_{sx}, τ_{sy}	components of surface shear stress	Nm^{-2}

τ_{xx} etc	components of stresses in vertical planes	Nm^{-2}
φ	direction of wave propagation	-

8. REFERENCES

1. ARTHUR, R.S., 1962
   A Note on the Dynamics of Rip Currents
   J. Geophys. Res., 67, 2777-2779

2. BOWEN, A.J., 1969
   Rip currents, 1, Theoretical Investigations
   J. Geophys. Res., 74, 5467-5478

3. DALRYMPLE, R.A., 1975
   A Mechanism for Rip Current Generation on an Open Coast
   J. Geophys. Res., 80, 3485-3487

4. GUSTAFSSON, B. and SUNDSTRÖM, A., 1978
   Incomplete parabolic problems in fluid dynamics
   SIAM, J. Appl. Math., 35, 2, 343-357

5. HINO, M., 1974
   Theory on Formation of Rip Current and Cuspidal Coast
   Proc. 14th Conf. Coast. Eng.

6. LeBLOND, P.H. and TANG, G.L., 1974
   On Energy Coupling between Waves and Rip Currents
   J. Geophys. Res., 79, 811-816

7. LIU, P.L.F. and MEI, C.C., 1976
   Watermotion on a beach in the presence of a breakwater, 2. Mean currents
   J. Geophys. Res., 81, 3085-3093

8. LONGUET HIGGINS, M.S., 1970
   Longshore Currents generated by Obliquely Incident Sea Waves, 2.
   J. Geophys. Res., 75, 6790-6801

9. MILLER, C.D., 1977
   Hydrodynamic instability in the surfzone and the formation of rip current gyres
   The Florida State University, Ph.D. 230 p.

10. SINGAMSETTI, S.R. and WIND, H.G., 1980
Breaking waves, characteristics of shoaling and breaking periodic waves normally incident to plane beaches of constant slope
Delft Hydraulics Laboratory, M 1371

11. SONU, C.J., 1972
Field Observation of Nearshore Circulation and Meandering Currents
J. Geophys. Res., 77, 3232-3247

12. Vreugdenhil, C.B., 1980
A Method of Computation for Unsteady Wave-driven Coastal Currents
Delft Hydraulics Laboratory, R 1174-part 1

	Fig.	wave conditions				geometry		
		H_o (m)	T (s)	φ	γ	beach slope	breaker line (m)	seaward boundary
set-up	1	1	5	0	0.766	0.025	57	100
longshore current (N=0)	3	1	5	30^o	0.766	0.025	53	200
longshore current (N=0.01)	4	1	5	30^o	0.766	0.025	53	200
longshore current (N=0.01)	5	1	5	30^o	0.766	0.025	53	200
circulation cells								
δ=0, N=0 , C=0.01	8	0.48	25	0	0.8	0.025	55	200
δ=0, N=0 , C=0.01	9	0.48	25	0	0.8	0.025	55	200
δ=0, N=0.01 , C=0.01	10	0.48	25	0	0.8	0.025	55	200
δ=1, N=0 , C=0.01	11	0.48	25	0	0.8	0.025	55	200
δ=1, N=0.01 , C=0.01	12	0.48	25	0	0.8	0.025	55	200
δ=1, N=0.01 , C=0	13	0.48	25	0	0.8	0.025	55	200
δ=1, N=0.01 , C=0	14	0.48	25	0	0.8	0.025	55	200
δ=1, N=0.033 , C=0	15	0.45	25	0	0.8	0.025	55	200
δ=1, N=0 , C=0.01	16	0.45	25	0	0.8	0.025	55	200
breakwaters	17	0.90	6	30^o	0.8	0.025	52	150
basin	18	0.90	6	30^o	0.8	0.025	52	150

Table 1 Wave conditions and geometry

	Fig.	Δx (m)	Δy (m)	number of grid points		Δt (s)	number of time steps		remarks
				x-dir.	y-dir.		n	Θ	
set-up	1	4	4	4	25	5	24	0.7	Δt,Δy variable
longshore current (N=0)	3	4	4-14	5	23	5	160	0.7	id.
longshore current (N=0.01)	4	4	4-14	5	23	5	160	0.7	id.
longshore current (N=0.01)	5	4	4-14	5	23	5	160	0.7	id.
circulation cells									
δ=0, N=0 , C=0.01	8	7,14	5-18	15	23	4	25	0.7	
δ=0, N=0 , C=0.01	9	7,14	5-18	15	23	4	25	0.7	
δ=0, N=0.01 , C=0.01	10	7,14	5-18	15	23	4	25	0.7	
δ=1, N=0 , C=0.01	11	7,14	5-18	15	23	4	25	0.7	
δ=1, N=0.01 , C=0.01	12	7,14	5-18	15	23	4	25	0.7	
δ=1, N=0.01 , C=0	13	7,14	5-18	15	23	4	25	0.7	
δ=1, N=0.01 , C=0	14	7,14	5-18	15	23	4	25	0.7	
δ=1, N=0.033 , C=0	15	7,14	5-18	15	23	4	25	0.7	
δ=1, N=0 , C=0.01	16	7,14	5-18	15	23	4	25	0.7	curved shoreline
breakwaters	17	10	5-18	11	23	4	25	0.7	
basin	18	10	5-18	11	23	4	25	0.7	

Table 2 Grid size, time step, etc.

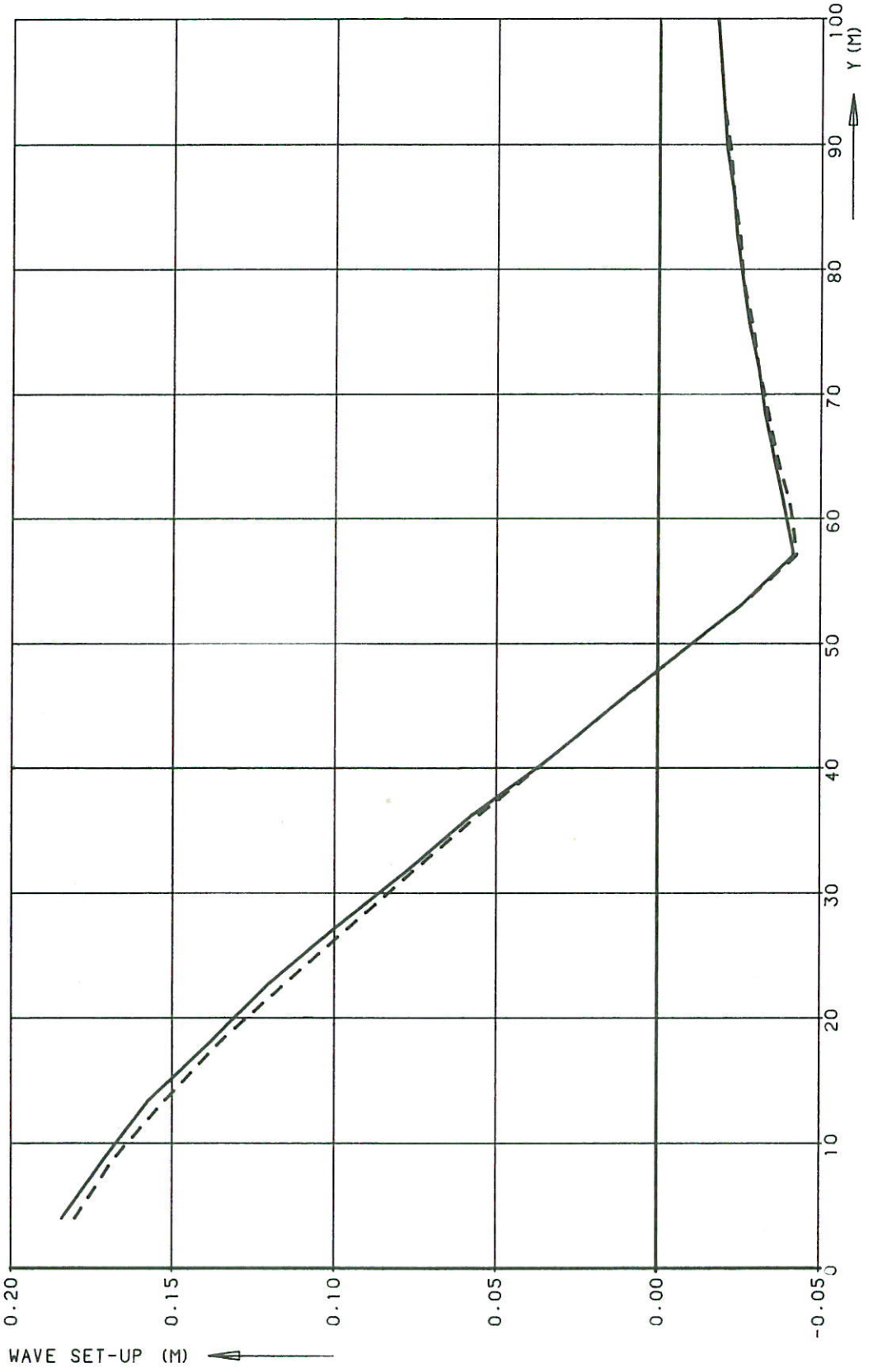

WAVE SET-UP

DELFT HYDRAULICS LABORATORY | R1174 | FIG. 1

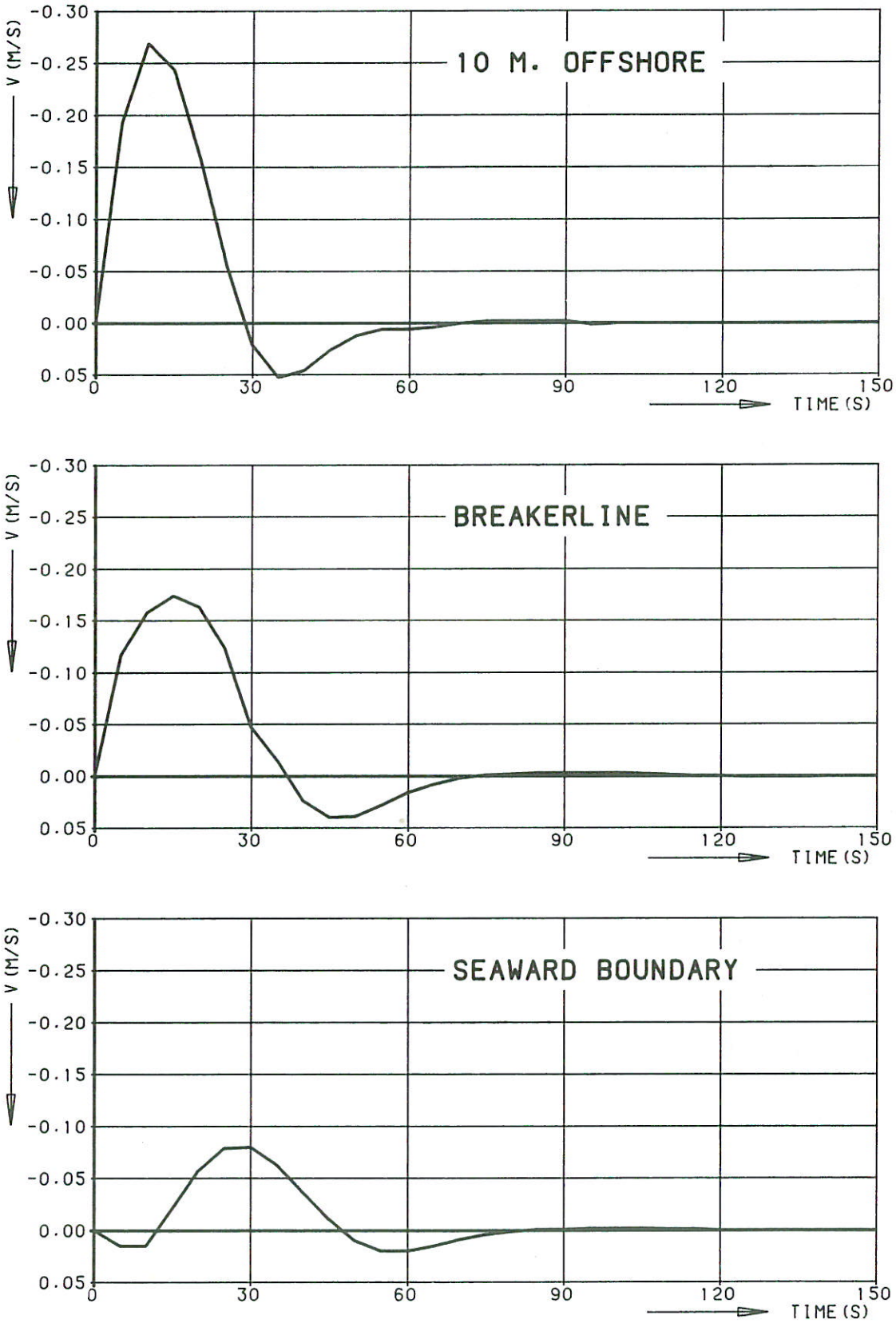

TIME FUNCTIONS OF THE VELOCITY NORMAL TO THE SHORE

DELFT HYDRAULICS LABORATORY | R1174 | FIG. 2

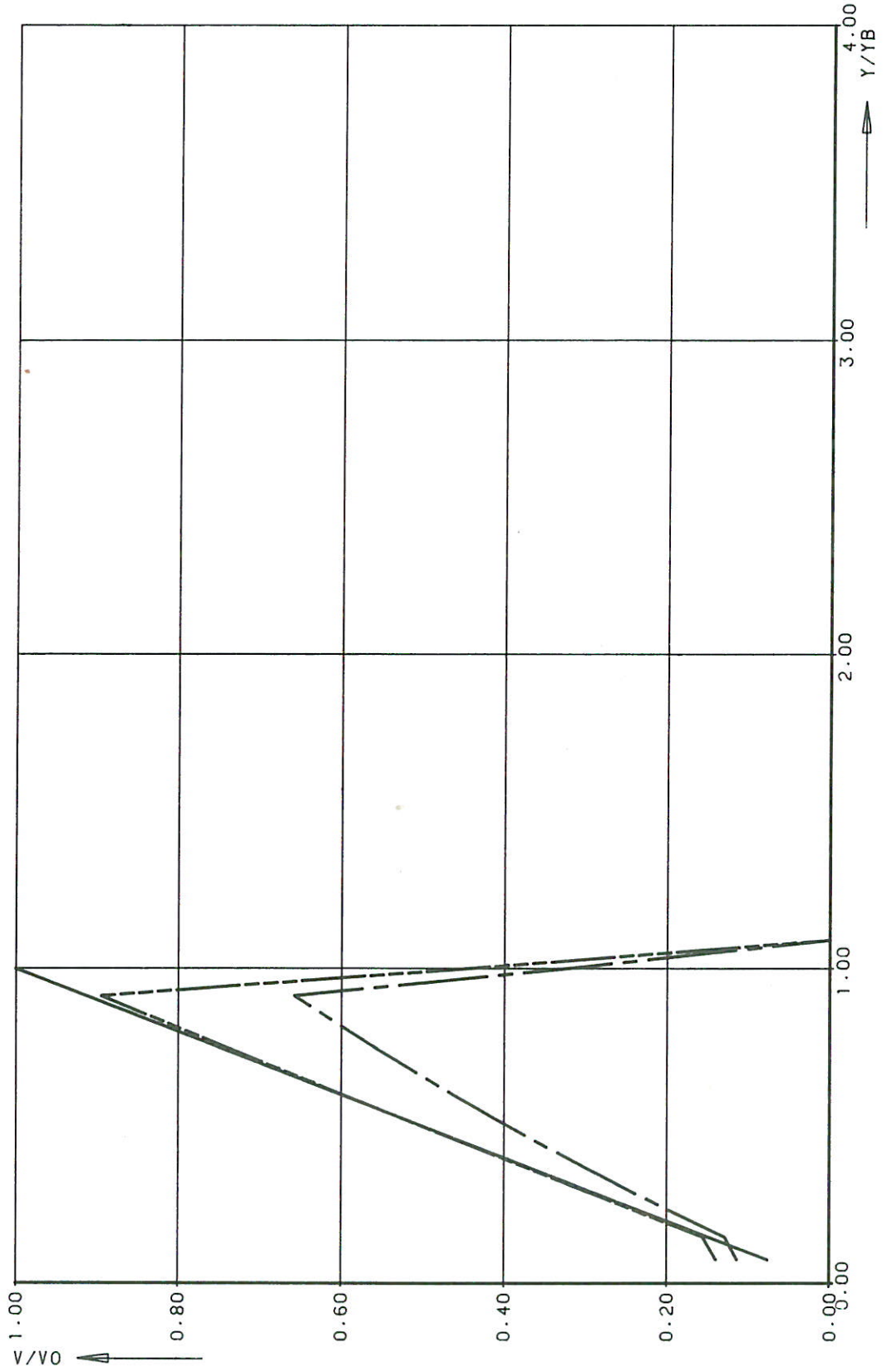

LONGSHORE VELOCITY DISTRIBUTION
WITH ZERO VISCOSITY

DELFT HYDRAULICS LABORATORY | R1174 | FIG. 3

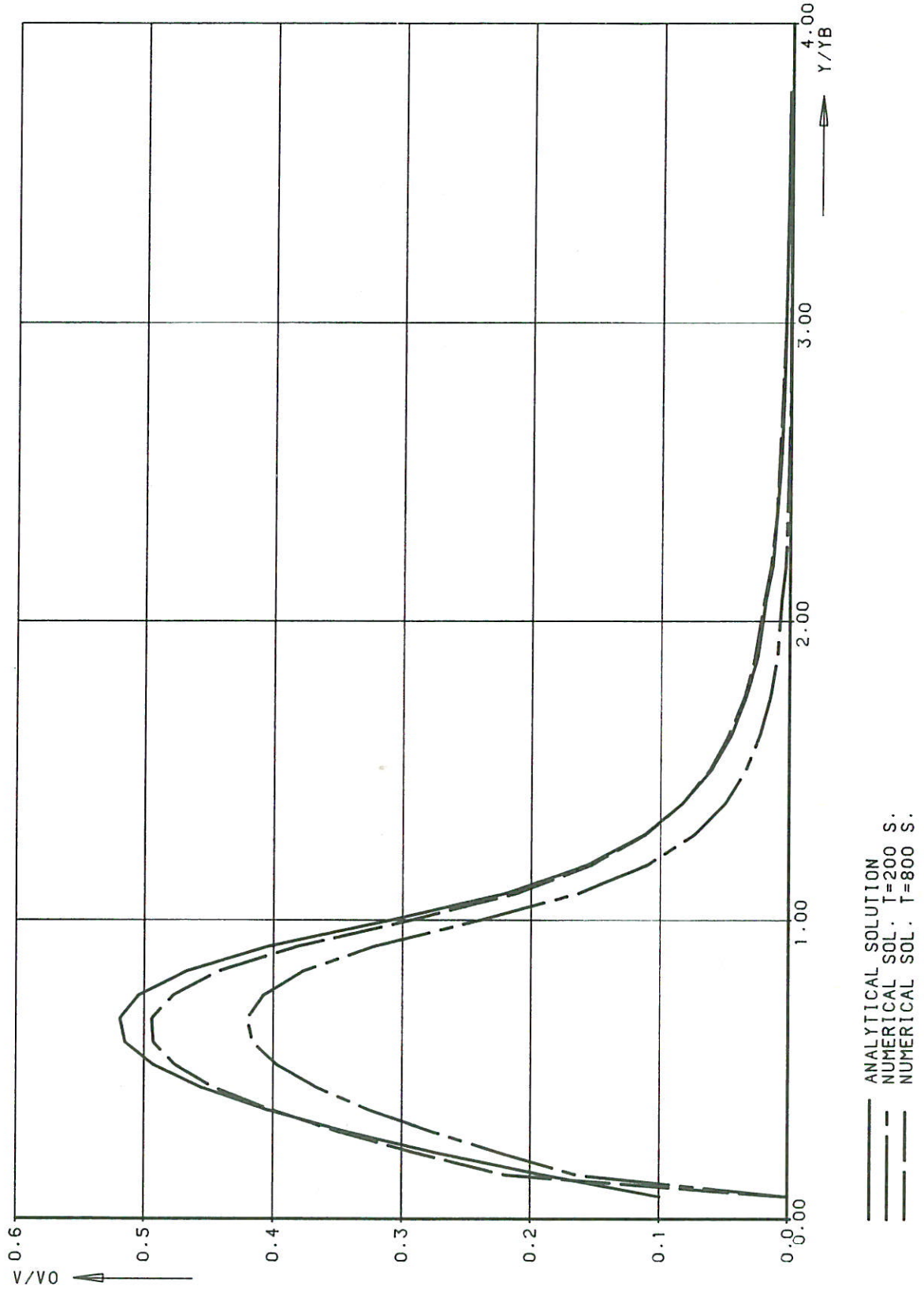

LONGSHORE VELOCITY DISTRIBUTION WITH V=0 AT THE SHORE AND AT THE SEAWARD BOUNDARY

DELFT HYDRAULICS LABORATORY | R1174 | FIG. 4

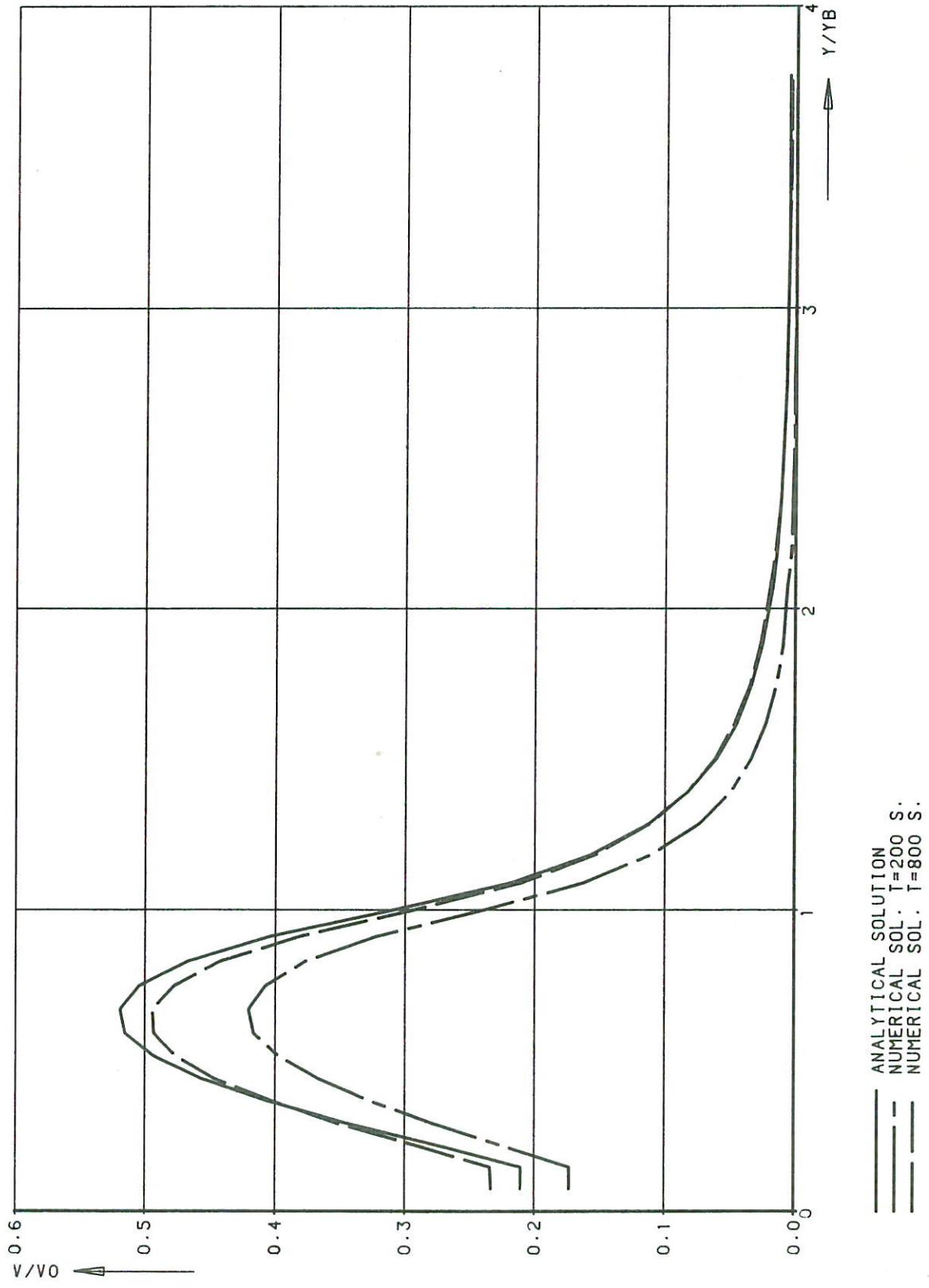

LONGSHORE VELOCITY DISTRIBUTION WITH DV/DY=0 AT THE SHORE AND AT THE SEAWARD BOUNDARY

DELFT HYDRAULICS LABORATORY | R1174 | FIG. 5

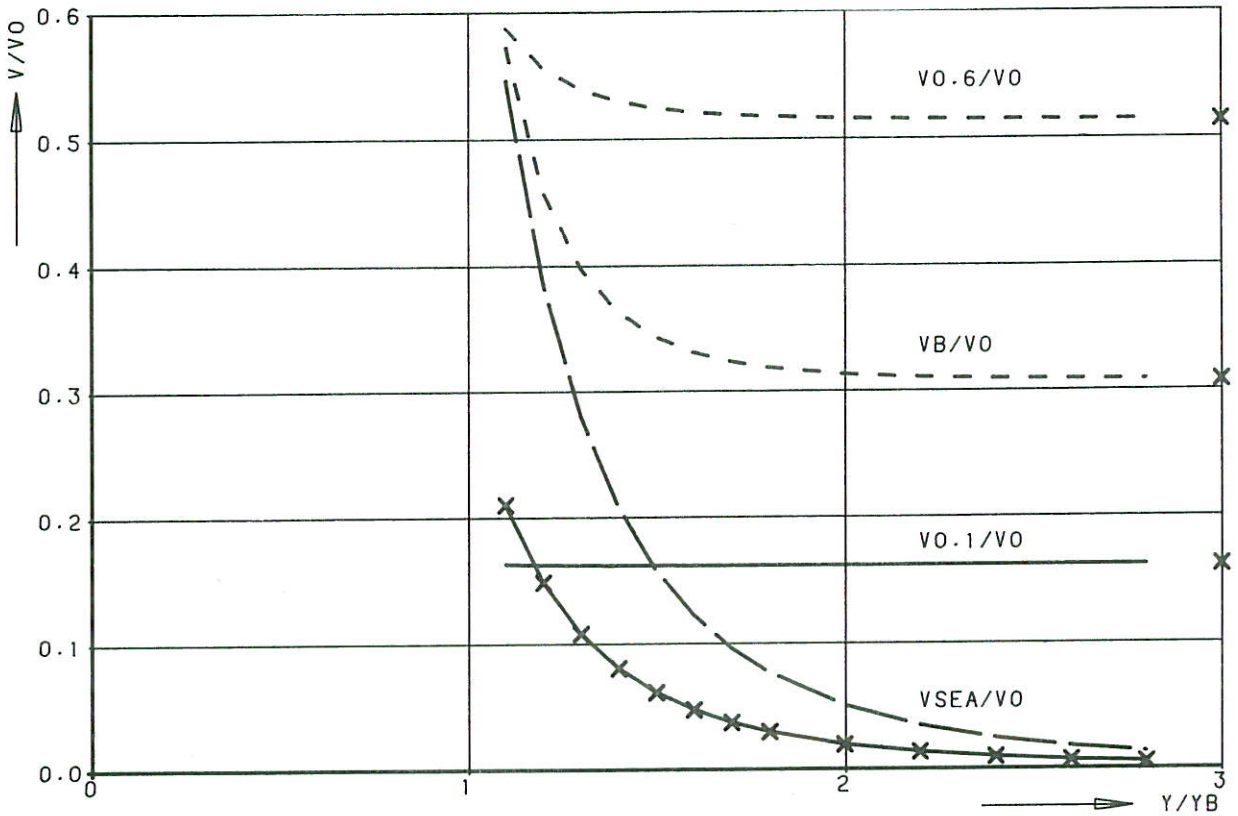

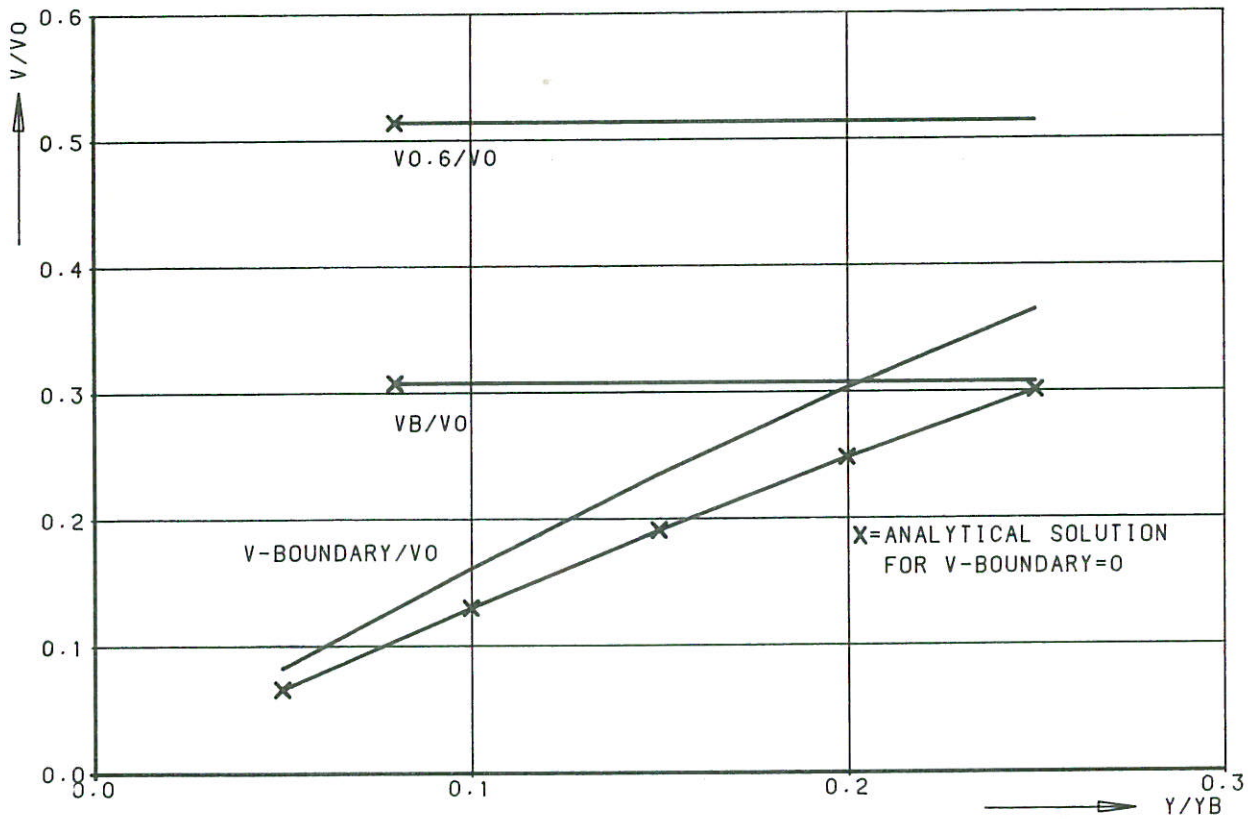

THE EFFECT OF THE POSITION OF THE BOUNDARY CONDITION DV/DY=0 ON THE VELOCITY PROFILE

DELFT HYDRAULICS LABORATORY | R1174 | FIG. 6

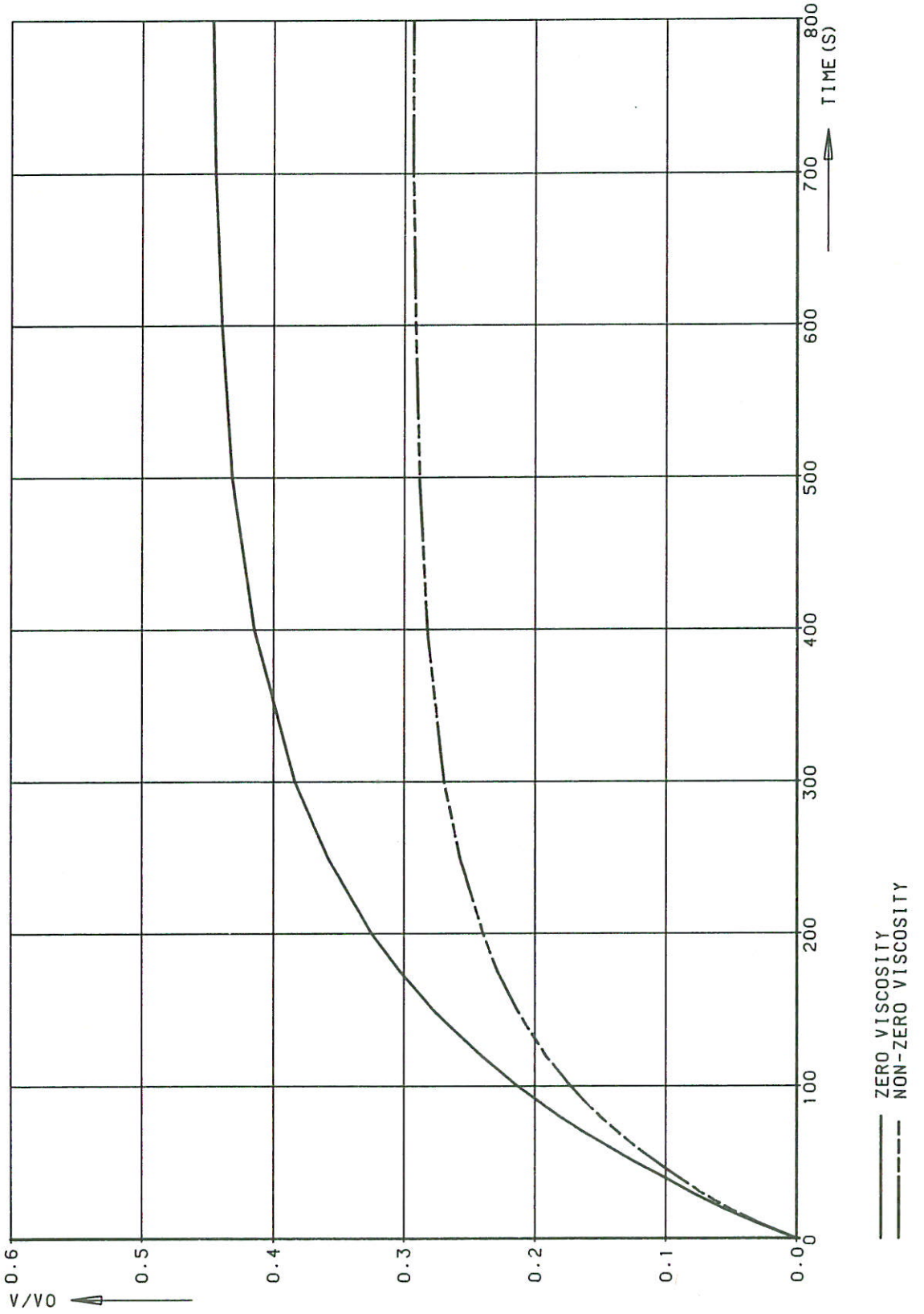

THE EVOLUTION OF THE LONGSHORE VELOCITY AT Y/YB= 1

DELFT HYDRAULICS LABORATORY | R1174 | FIG. 7

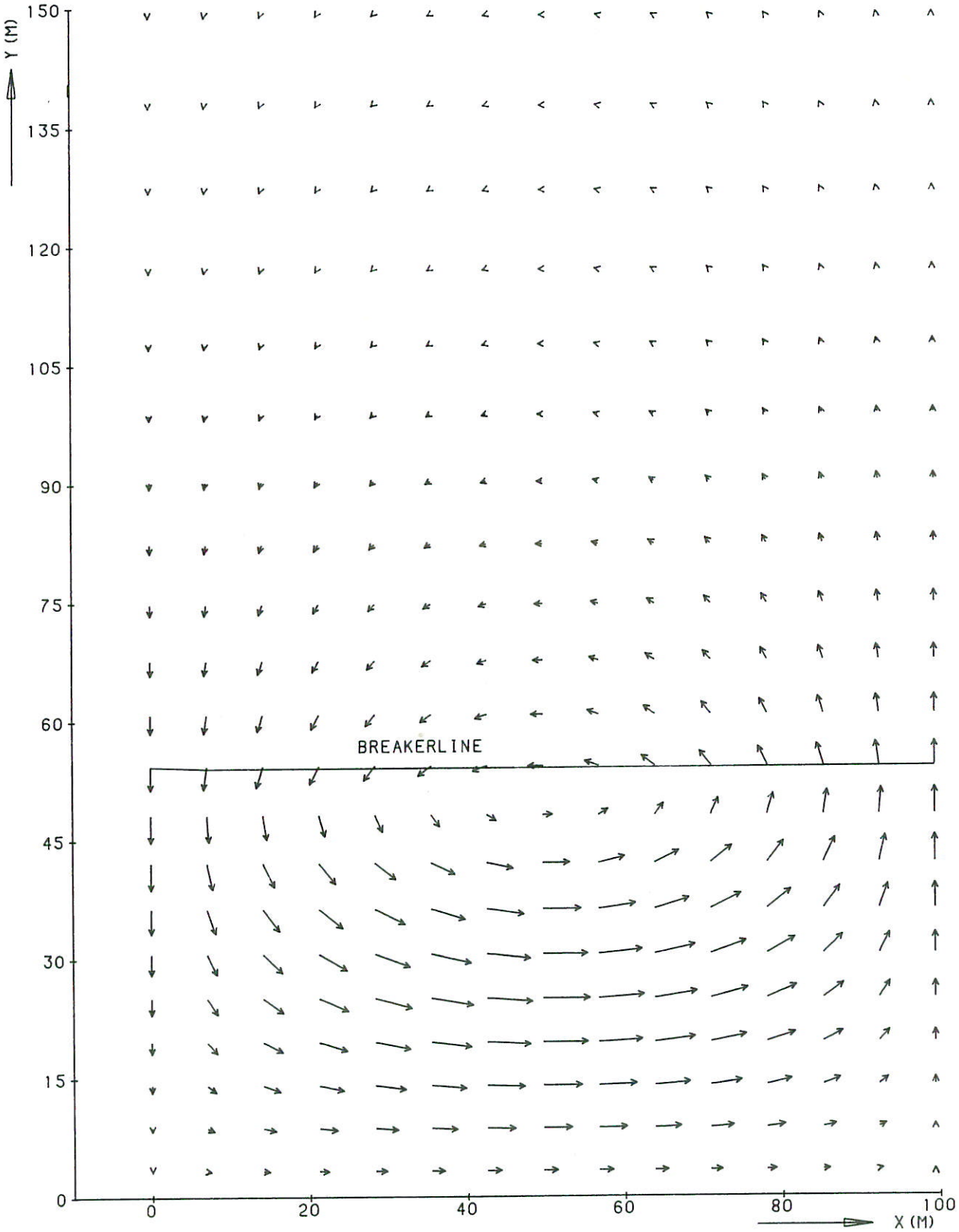

VELOCITY SCALE 1 CM = 0.20 M/S

CIRCULATION CELLS
ANALYTICAL SOLUTION WITHOUT BOTH VISCOSITY AND CONVECTIVE TERMS

DELFT HYDRAULICS LABORATORY | R1174 | FIG. 8

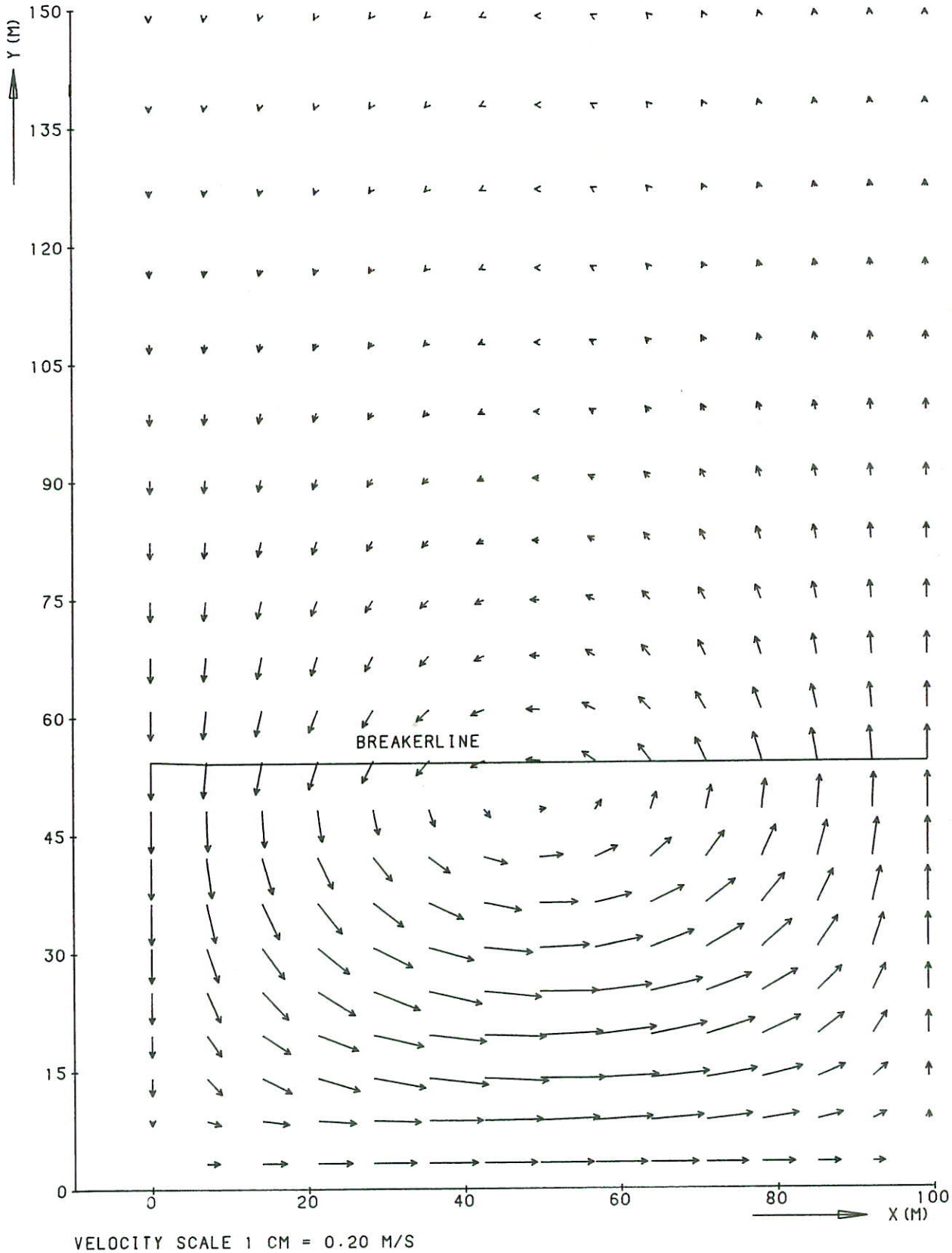

CIRCULATION CELLS
NUMERICAL SOLUTION WITHOUT BOTH VISCOSITY AND CONVECTIVE TERMS

DELFT HYDRAULICS LABORATORY | R1174 | FIG. 9

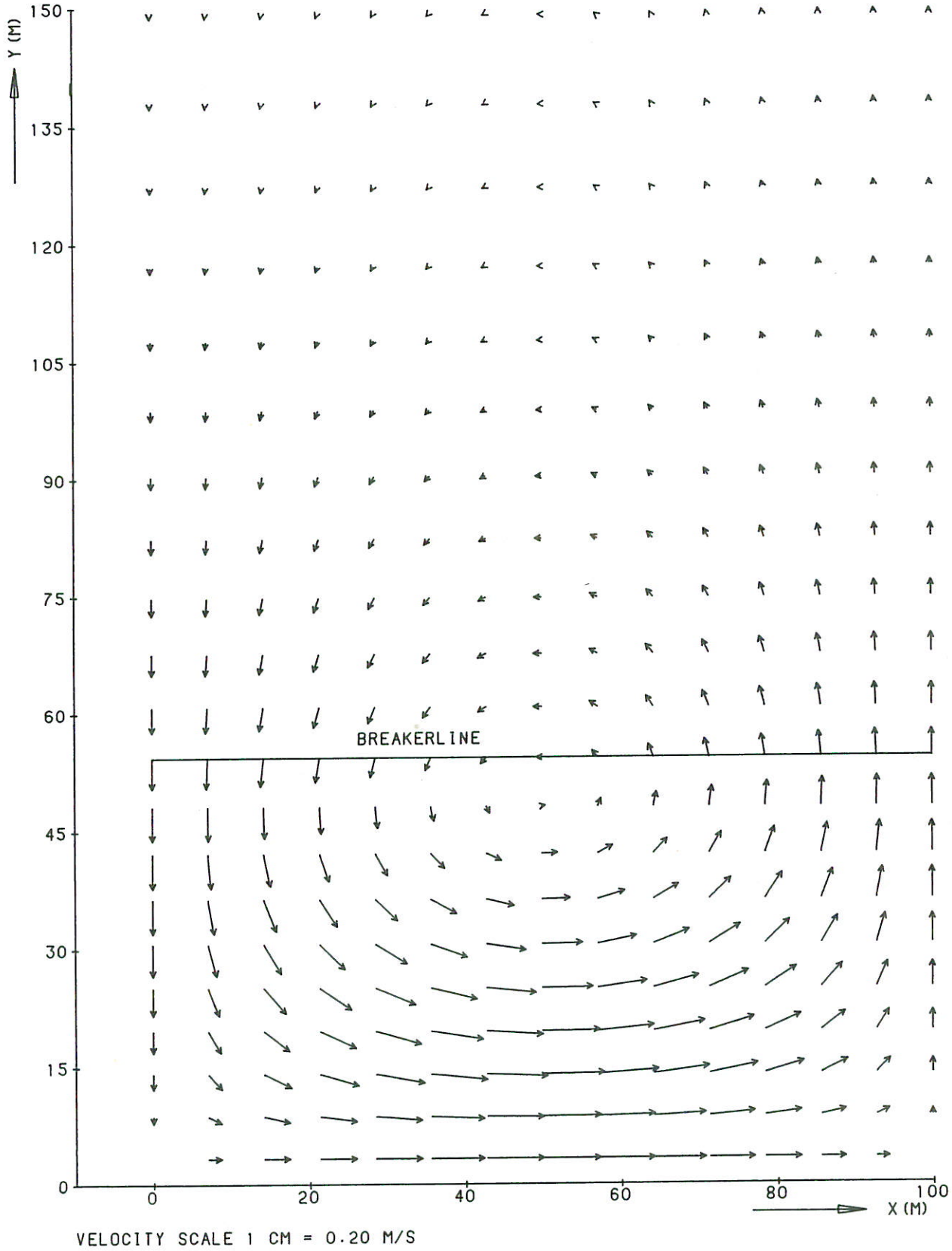

CIRCULATION CELLS
NUMERICAL SOLUTION FOR RE = 0

DELFT HYDRAULICS LABORATORY | R1174 | FIG. 10

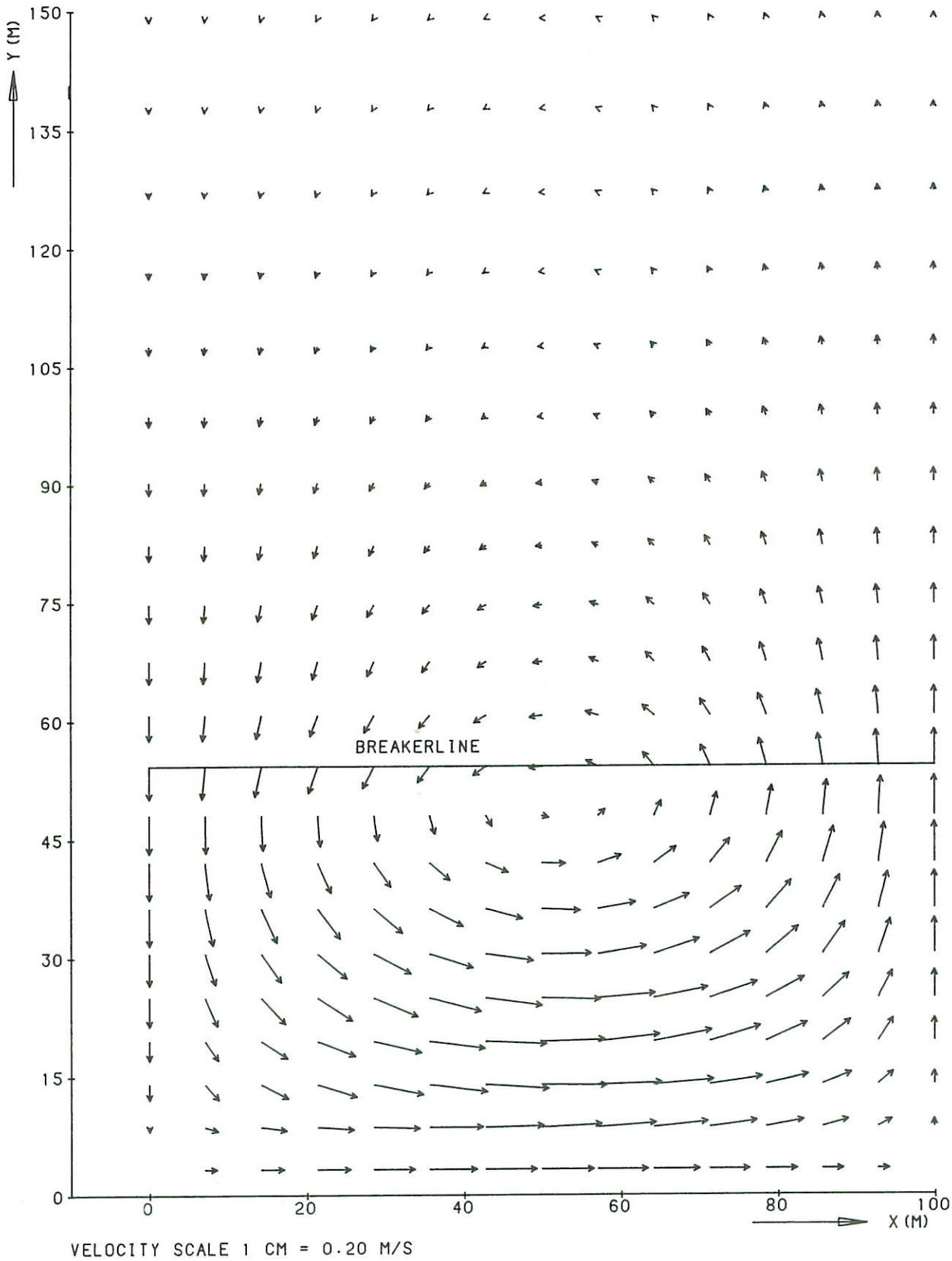

CIRCULATION CELLS
NUMERICAL SOLUTION FOR RE = INFINITE

DELFT HYDRAULICS LABORATORY | R1174 | FIG. 11

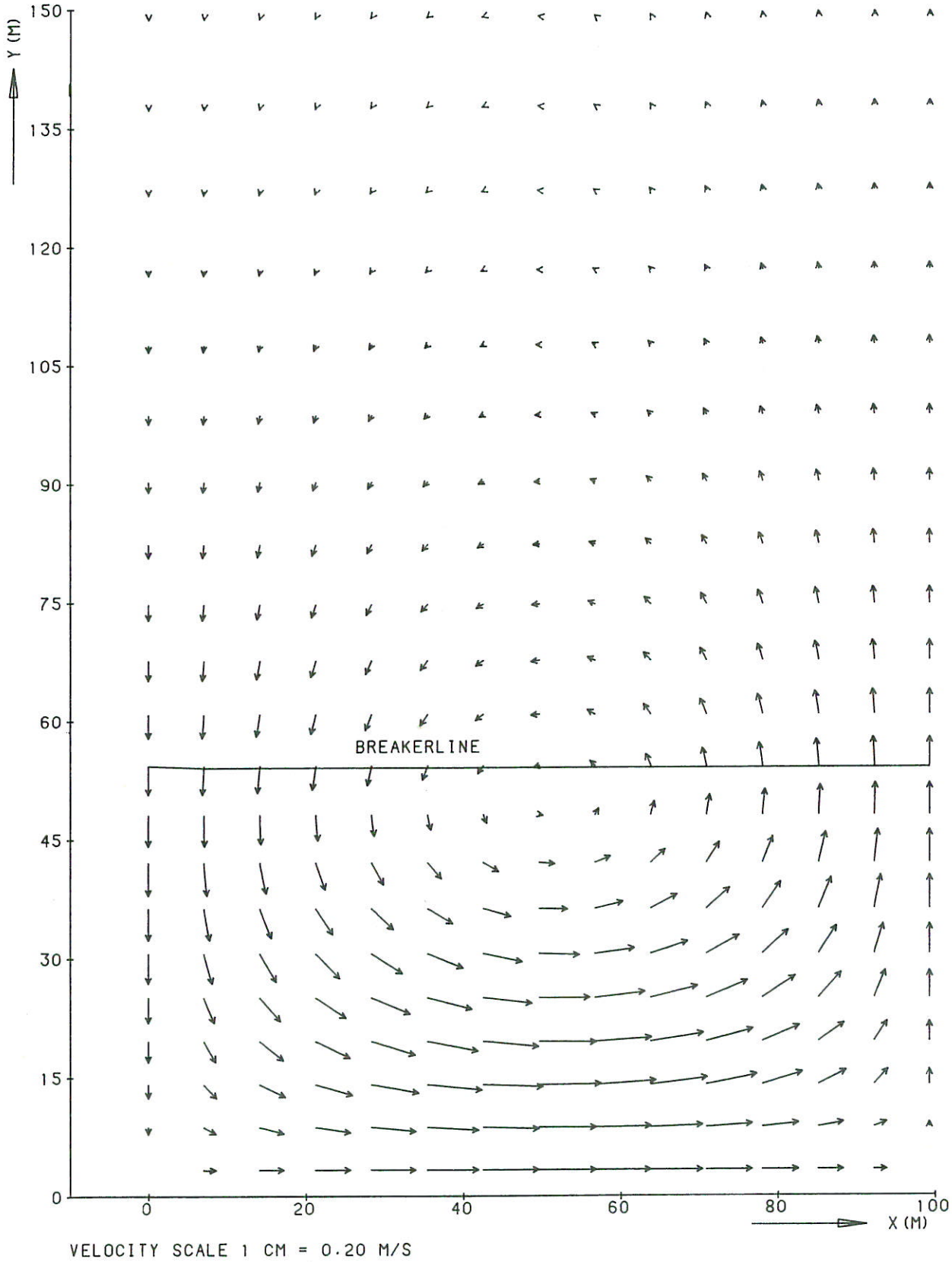

CIRCULATION CELLS
NUMERICAL SOLUTION FOR RE = 3

DELFT HYDRAULICS LABORATORY | R1174 | FIG. 12

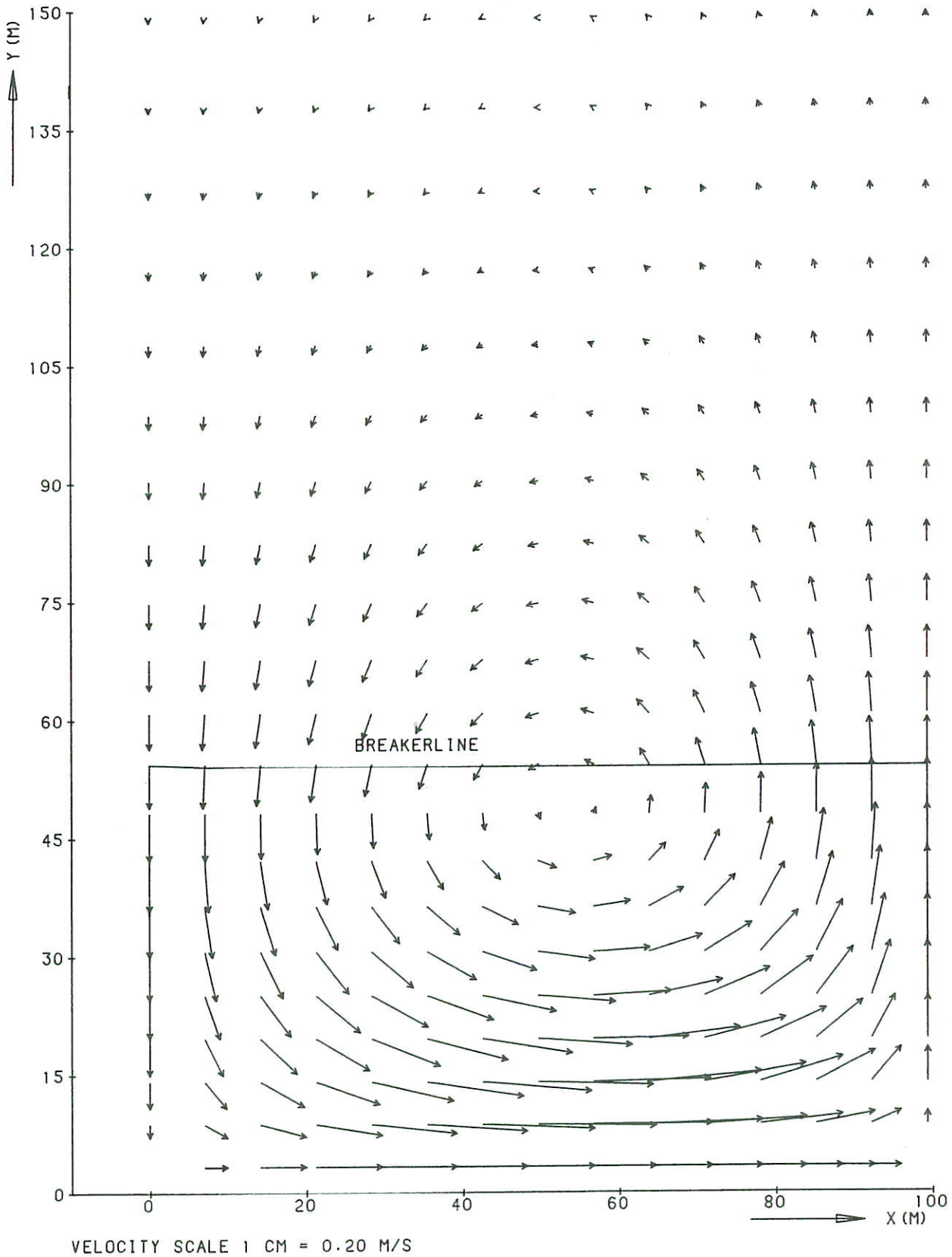

CIRCULATION CELLS
NUMERICAL SOLUTION FOR RE = 3
BOTTOMFRICTION IS ZERO

DELFT HYDRAULICS LABORATORY | R1174 | FIG. 13

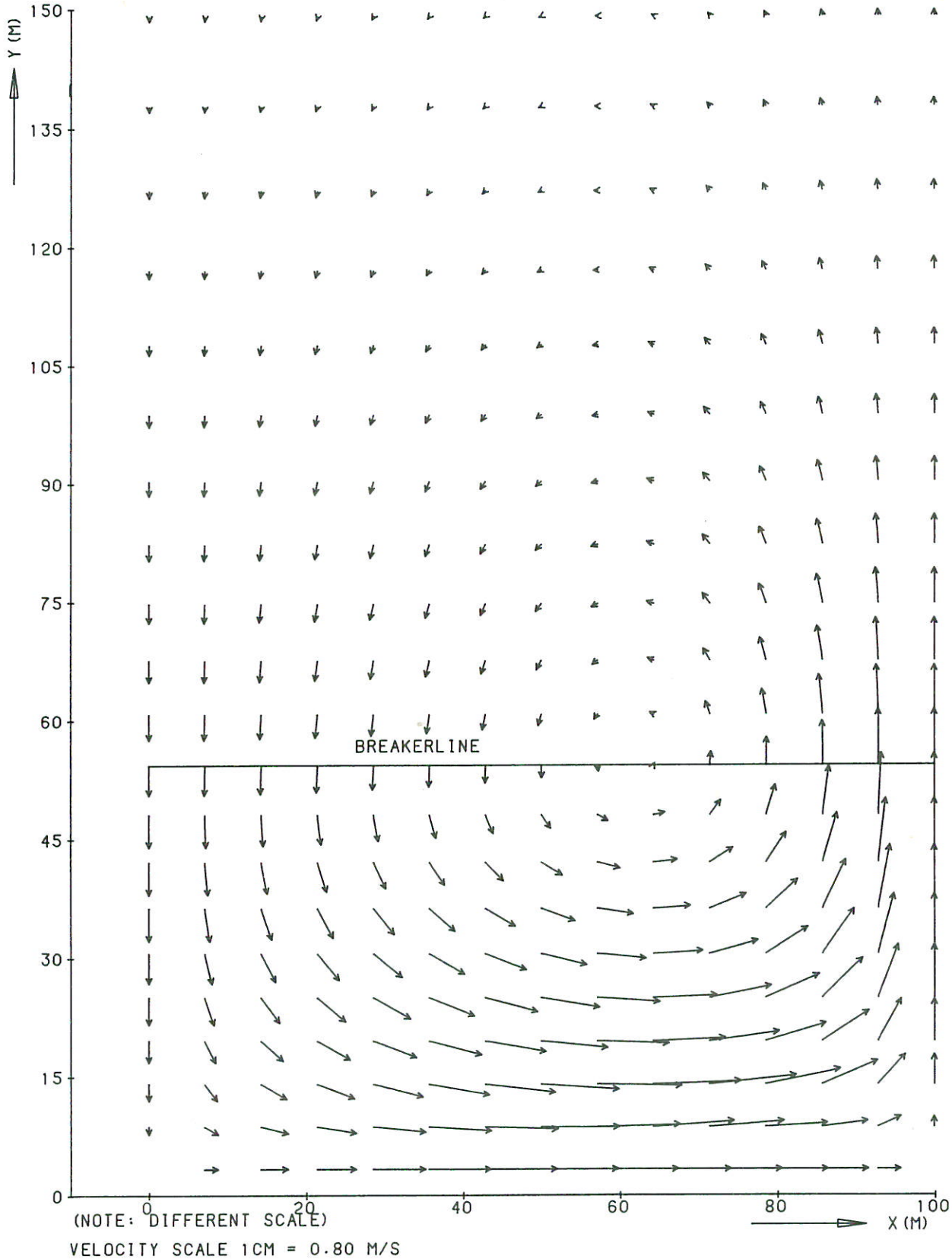

CIRCULATION CELLS
NUMERICAL SOLUTION FOR RE = 9
BOTTOMFRICTION IS ZERO

DELFT HYDRAULICS LABORATORY | R1174 | FIG. 14

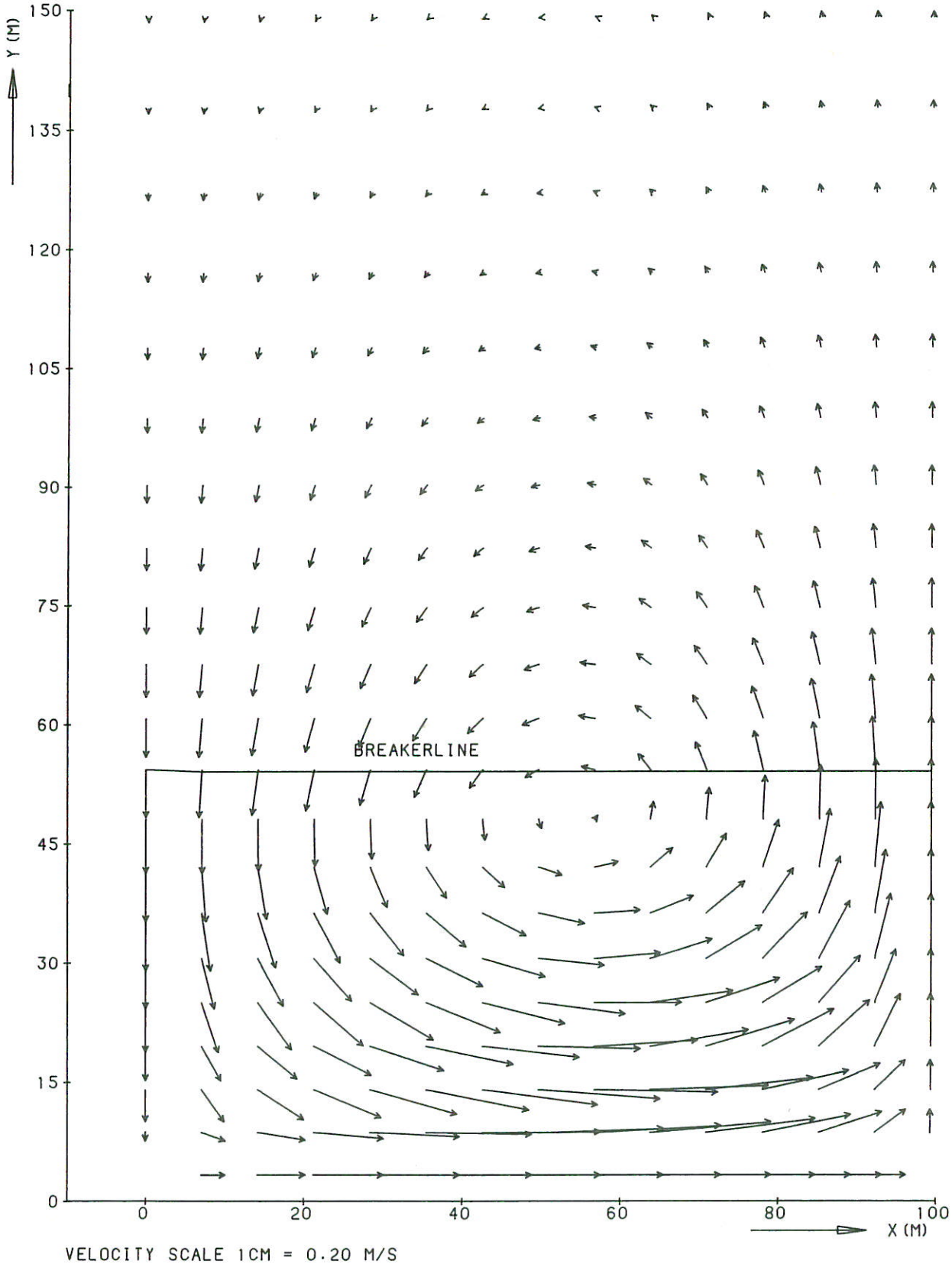

CIRCULATION CELLS
NUMERICAL SOLUTION FOR RE = 9
REDUCED VISCOSITY (N = .01/3)

DELFT HYDRAULICS LABORATORY | R1174 | FIG. 15

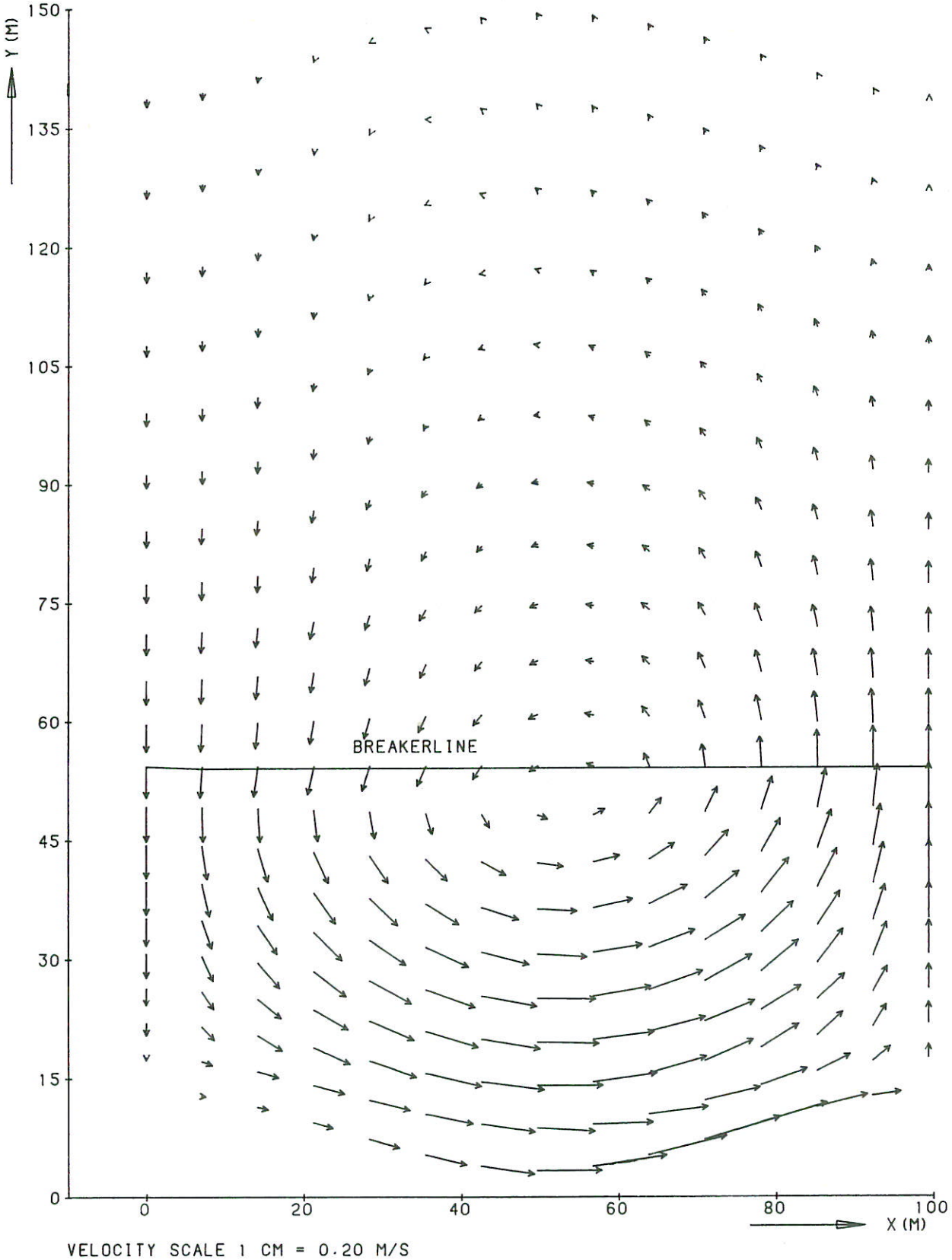

CIRCULATION CELLS
NUMERICAL SOLUTION FOR RE = INFINITE CURVED SHORELINE

DELFT HYDRAULICS LABORATORY | R1174 | FIG. 16

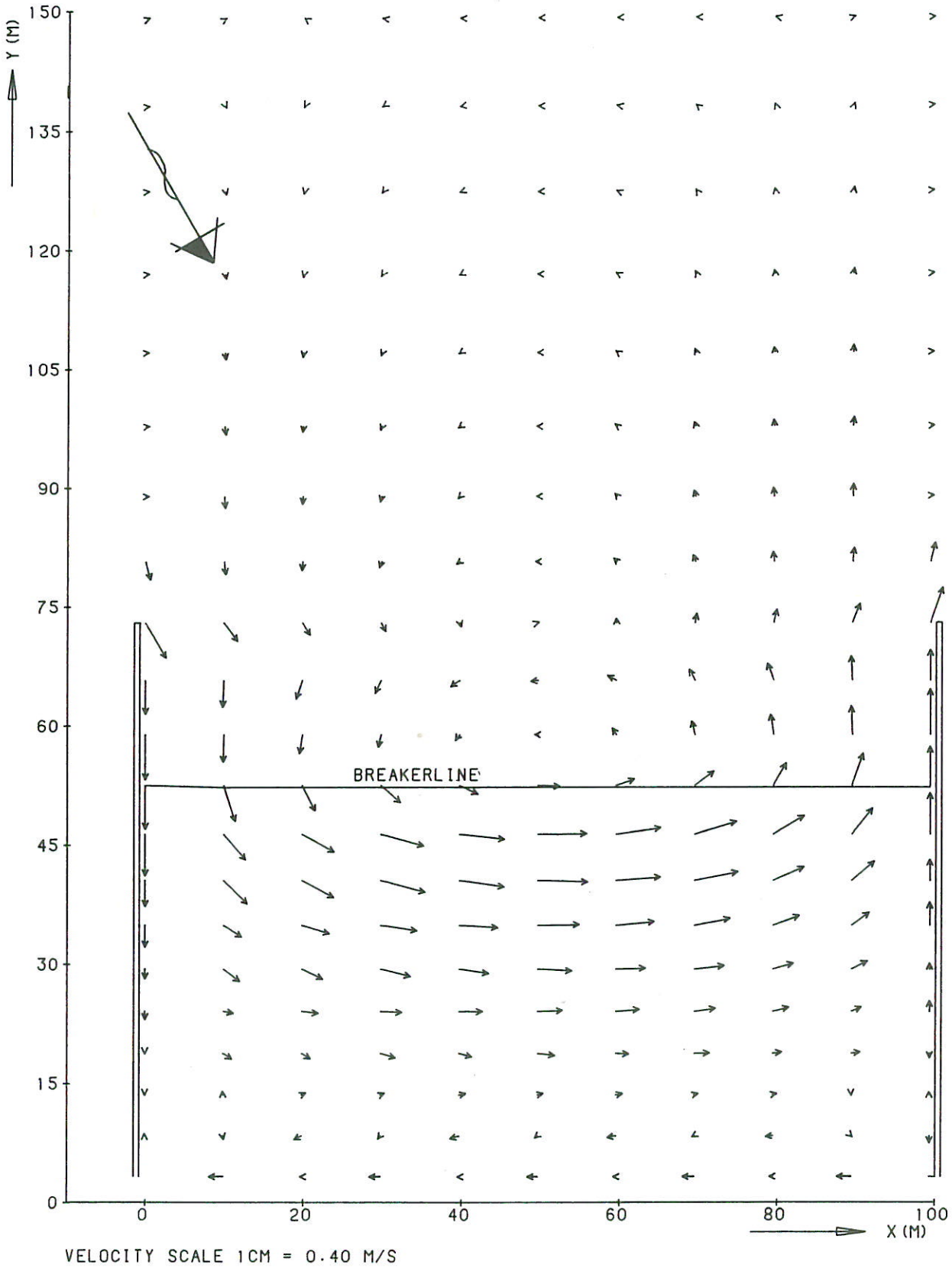

WAVE DRIVEN CURRENTS
AROUND BREAKWATERS

DELFT HYDRAULICS LABORATORY | R1174 | FIG. 17

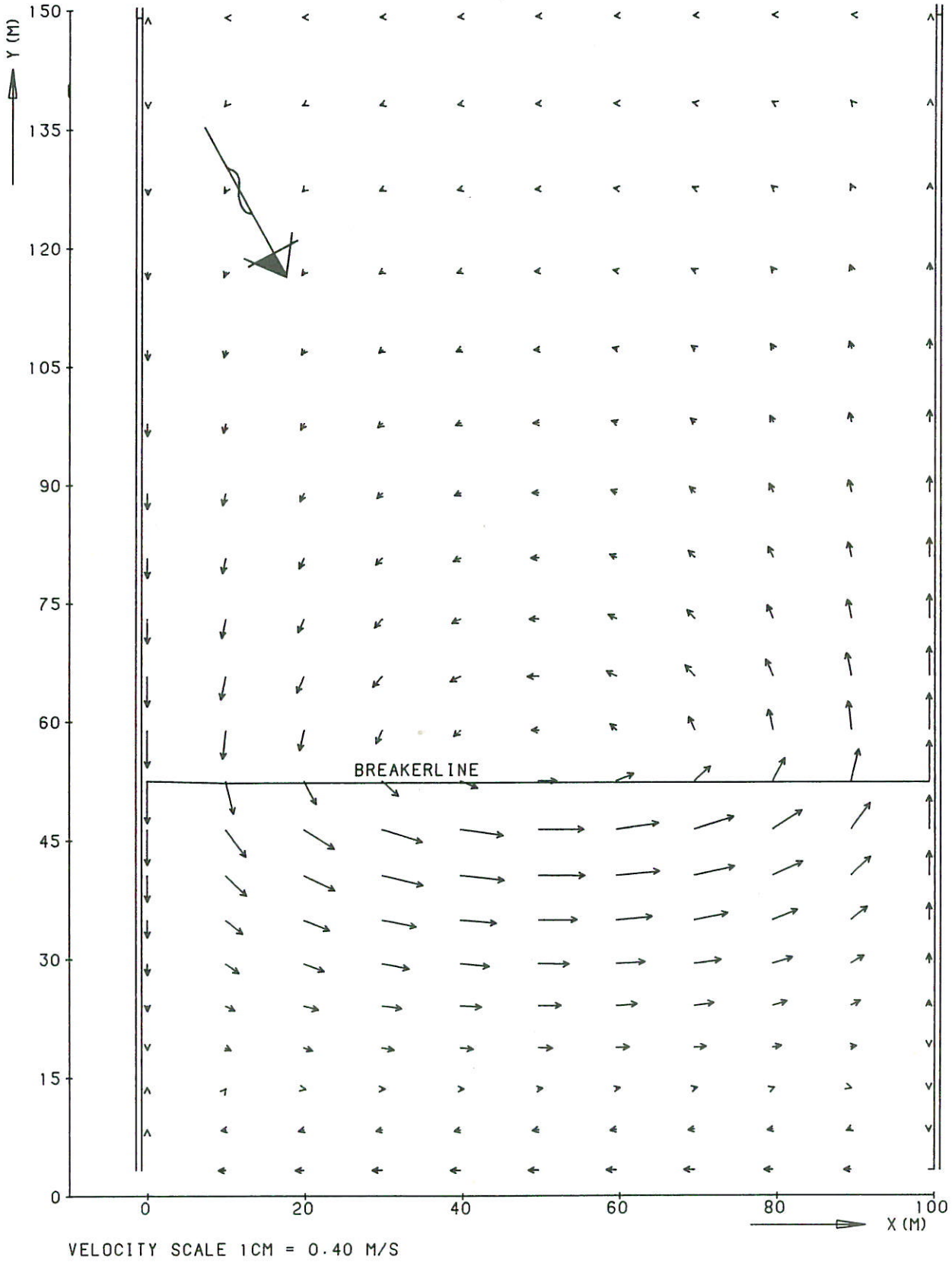

WAVE DRIVEN CURRENTS
IN A CLOSED BASIN

DELFT HYDRAULICS LABORATORY | R1174 | FIG. 18

APPENDIX A BRIEF DESCRIPTION OF THE MODEL

The equations of the mathematical model for unsteady wave driven coastal currents averaged over depth and wave period are presented and discussed in [12]. Here only a summary will be given. The continuity equation and the two momentum equations are:

$$\frac{\partial h}{\partial t} + \frac{\partial p}{\partial x} + \frac{\partial q}{\partial y} = 0 \qquad (A.1)$$

$$\frac{\partial p}{\partial t} + \frac{\partial}{\partial x}(p^2/h) + \frac{\partial}{\partial y}(pq/h) + gh\left(\frac{\partial h}{\partial x} + \frac{\partial z_b}{\partial x}\right) + \\ - \tau_{sx}/\rho + \tau_{bx}/\rho + \frac{1}{\rho}\left(\frac{\partial S_{xx}}{\partial x} + \frac{\partial S_{xy}}{\partial y}\right) - \frac{1}{\rho}\left(\frac{\partial h\tau_{xx}}{\partial x} + \frac{\partial h\tau_{xy}}{\partial y}\right) = 0 \qquad (A.2)$$

$$\frac{\partial q}{\partial t} + \frac{\partial}{\partial x}(pq/h) + \frac{\partial}{\partial y}(q^2/h) + gh\left(\frac{\partial h}{\partial y} + \frac{\partial z_b}{\partial y}\right) - \tau_{sy}/\rho + \\ + \tau_{by}/\rho + \frac{1}{\rho}\left(\frac{\partial S_{xy}}{\partial x} + \frac{\partial S_{yy}}{\partial y}\right) - \frac{1}{\rho}\left(\frac{\partial h\tau_{xy}}{\partial x} + \frac{\partial h\tau_{yy}}{\partial y}\right) = 0 \qquad (A.3)$$

where:

h	= mean water depth	m
p,q	= volume transport in x- and y-direction	m^2/s
g	= acceleration due to gravity	ms^{-2}
z_b	= bottom level above reference level	m
τ_{sx},τ_{sy}	= shear stress at the surface	N/m^2
τ_{bx},τ_{by}	= bottom shear stress	N/m^2
ρ	= fluid density	kg/m^3
S_{xx} etc	= components of the radiation stress	N/m^2
τ_{xx} etc	= components of the effective stress	N/m^2

For the wave field the linear wave approximations have been used. For a slowly varying wave field the resulting radiation stresses are (Longuet Higgins 1964):

$$S_{xx} = E\,(n\cos^2\varphi + n - \tfrac{1}{2}) \qquad (A.4)$$

$$S_{xy} = E\,n\sin\varphi\cos\varphi \qquad (A.5)$$

$$S_{yy} = E\,(n\sin^2\varphi + n - \tfrac{1}{2}) \qquad (A.6)$$

where $E = \frac{1}{8} \rho g H^2$ (A.7)

H = local wave height

φ = angle between direction of wave propagation and x-axis

$n = \frac{1}{2} + kh/(\sinh 2kh)$

Inside the breaker zone the wave height is determined by the breaker index γ

$\gamma = H/d$

where d is the still water depth. It is also possible to restart the programme after changing the wave field according to the calculated mean water level. In this report this procedure has not been applied.

For the definition of the horizontal momentum exchange care has been taken of the fact that this definition must not depend on the choice of the coordinate system. The following definitions have been chosen (see [12])

$$\tau_{xx}/\rho = \varepsilon \{\frac{\partial}{\partial x} (p/h) - \frac{\partial}{\partial y} (q/h)\} \quad (A.8)$$

$$\tau_{xy}/\rho = \varepsilon \{\frac{\partial}{\partial y} (p/h) + \frac{\partial}{\partial x} (q/h)\} \quad (A.9)$$

$$\tau_{yy}/\rho = \varepsilon \{\frac{\partial}{\partial y} (q/h) - \frac{\partial}{\partial x} (p/h)\} \quad (A.10)$$

For the value of ε various approximations can be used.

The bottom shear stresses τ_{bx} and τ_{by} are linear in terms of the mean flow p,q.

$$\frac{1}{\rho} (\tau_{bx}, \tau_{by}) = \frac{r}{h}(p,q) \quad (A.11)$$

where r is a dimensional frictional coefficient equivalent to $c_f |u_{orb}|$. Also for r different expressions can be applied. In this report the definition of Bowen (1969) has been used in Figures 8 and 9. To the remaining cases the definition of Longuet Higgins (1970) has been applied. In future research also definitions of r will be used, such as the inherent anisotropy of r in the definition of Longuet Higgins and the work of Jonsson.

APPENDIX B LONGSHORE CURRENTS

Longuet Higgins (1970) has derived a longshore current distribution for oblique incident waves on a plane beach. In order to obtain a tractable problem he introduced the following assumptions:

a shallow water approximation of the linear wave theory
b bottom friction can be described by

$$\frac{1}{\rho}\bar{\tau}_{bx} = (\gamma c/(gh)^{\frac{1}{2}}.U)/\pi \qquad (B.1)$$

c lateral mixing coefficient ε can be written as:

$$\varepsilon = N \quad |y| \quad (gh)^{\frac{1}{2}} \qquad (B.2)$$

Furthermore the momentum balance parallel to the shoreline (see (A.2)) is made dimensionless by means of the parameter Y_B, the width of the breaker zone, and U_o, the current velocity at the breaker line when lateral mixing is absent:

$$U_o = (5.\pi.\gamma.\ (gh_B)^{\frac{1}{2}}.m.\sin\varphi_B)/(16C) \qquad (B.3)$$

The indices B are referring to the value of the parameters at the breaker line.

The resulting equations are:

$$P\frac{\partial}{\partial y}\ (y^{5/2}\ \frac{\partial u}{\partial y}) - y^{1/2}.u + y^{3/2} = 0 \qquad 0 < y < 1 \qquad (B.4)$$

$$P\frac{\partial}{\partial y}\ (y^{5/2}\ \frac{\partial u}{\partial y}) - y^{1/2}.u = 0 \qquad 1 < y < \infty \qquad (B.5)$$

$$u = U/U_o \qquad (B.6)$$

$$y = Y/Y_B \qquad (B.7)$$

$$P = (\pi.m.N)/(\gamma.C) \qquad (B.8)$$

The factor P represents the ratio between the coefficient of the dimensionless lateral mixing term and the coefficient of the dimensionless bottom friction term.

The solution of B1 and B2 except for P = 0.4 is

$$u = B1\ y^{P1} + Ay \qquad 0 < y < 1 \qquad (B.9)$$

$$u = B2\ y^{P2} \qquad 1 < y < \infty \qquad (B.10)$$

$$P1 = -3/4 + (9/16 + 1/P)^{\frac{1}{2}} \qquad (B.11)$$

$$P2 = -3/4 + (9/16 + 1/P)^{\frac{1}{2}} \qquad (B.12)$$

$$A = 1/(1-5P/2) \qquad (B.13)$$

$$B1 = A(P2-1)/(P1-P2) \qquad (B.14)$$

$$B2 = A(P1-1)/(P1-P2) \qquad (B.15)$$

This solution satisfies the boundary condition U=0 both at the shoreline and in infinity.

However, in the computer programme RIPCEL the boundary conditions are in case of non-zero viscosity:

$$\frac{\partial u}{\partial y} = 0 \qquad y = y_{shore} \qquad y=y_{sea} \qquad (B.16)$$

in which y_{shore} and y_{sea} are the dimensionless distances of the first grid point near the shoreline and the position of the seaward boundary respectively.

A solution of B4 in this case is

$$u = Ay + By^{P1} + Cy^{P2} \qquad 0 < y < 1 \qquad (B.17)$$

The term Ay is a particular integral of B4, of which

$$A = 1/(1-5P/2) \qquad (B.18)$$

A solution of B5 is

$$u = Dy^{P1} + Ey^{P2} \qquad 1 < y < \infty \qquad (B.19)$$

Continuity of both velocity and velocity gradient at the breaker line yields from B17 and B19

$$A + B + C = D + E \tag{B.20}$$

$$A + BP_1 + CP_2 = DP_1 + EP_2 \tag{B.21}$$

The free-slip condition near the shore and at the seaward boundary yields the following equations

$$A + BP_1 y_{shore}^{P_1-1} + CP_2 y_{shore}^{P_2-1} = 0 \tag{B.22}$$

$$DP_1 y_{sea}^{P_1-1} + EP_2 y_{sea}^{P_2-1} = 0 \tag{B.23}$$

From the equations (B.20) through (B.23) the constants B through E have to be determined.